

pubs.acs.org/acscatalysis Research Article

Elucidating the Roles of Distinct Chemical Factors in the Hydrolytic Activities of Hetero- and Homonuclear Synthetic Analogues of Binuclear Metalloenzymes

Vindi M. Jayasinghe-Arachchige, Leonardo F. Serafim, Qiaoyu Hu, Cihan Ozen, Sreerag N. Moorkkannur, Gerhard Schenk, and Rajeev Prabhakar*



Cite This: ACS Catal. 2023, 13, 3131-3147



ACCESS I

III Metrics & More

Article Recommendations

Supporting Information

ABSTRACT: In this study, hydrolytic activities of hetero- and homobinuclear metallovariants of an asymmetric (I) or symmetric (II) ligand with the Fe^{III} - Zn^{II} , Zn^{II} - Zn^{II} , and Cu^{II} - Cu^{II} cores (*i.e.*, I_{FZ} , I_{ZZ} , and I_{CC} or I_{FZ} , I_{IZZ} , and I_{CC} respectively) are investigated using DFT calculations through four distinct mechanisms: dissociative (DA), substrate-assisted (SA), water-assisted (WA), and associative (AS). Additionally, the effects of different nucleophiles (μ -OH, terminal-OH, and - O_2H_3), coordination numbers, *para* substituents (-CH₃, -Cl, and -NO₂) of the linker, and an external electric field on the energetics of these reactions are computed. The geometries, spin ground states, and substrate binding modes of the three metal centers for both asymmetric (I) and symmetric (II) ligands differ from each other. There is no Lewis acid activation of the bis(2,4-dinitrophenyl) phosphate (BDNPP) substrate, and hydrolysis is predominantly



controlled by the nucleophilicity of the metal-bound hydroxyl ion. The electronic nature of the metal ions determines the activities of their complexes, and the homobinuclear I_{ZZ} is found to be the most active complex. However, complexes formed with ligand I are not more active than their ligand-II-containing counterparts for all metal ions. The DFT calculations suggest that the DA pathway is the energetically most feasible among the four pathways. The terminal hydroxyl group is the strongest nucleophile, and the electron-donating -CH₃ group is the most suitable *para* substituent in the linker. Whereas the introduction of an external electric field along the reaction axis lowers the barrier for I_{FZ} , it leaves that unchanged for I_{ZZ} and increases that for I_{CC} . These combined results in this study highlight the influence of distinct critical chemical factors such as the electronic nature of the metal ions, the ligand environment, as well as the linker and nucleophile on phosphoester hydrolysis. Insights gained will guide the design of the next generation of versatile metal complexes for a wide range of reactions and applications.

KEYWORDS: hydrolysis, binuclear complexes, chemical factors, synthetic analogues, reaction mechanisms, electric field and phosphodiester

1. INTRODUCTION

In the last few decades, a wide range of binuclear metal complexes have been developed to catalyze diverse chemical reactions. These complexes were largely inspired by the hetero- and homobinuclear metal centers of natural enzymes. Despite the impressive advances made in the field, the ultimate goal of designing efficient enzyme mimics is still elusive. Currently, metal complexes exhibit much slower activities and lower turnover numbers in comparison to the natural enzymes. Thus, there is an intense interest in designing the next generation of molecules with improved activities. The realization of this aim will require a deeper understanding of diverse chemical factors that influence their activities. In general, the design of an efficient metal complex mimic requires a productive combination of metal ions, hydrophobic groups, hydrogen bond donating moieties, metal

chelates, and organic functional groups on the ligand. Additionally, it needs to preserve the following key features of enzymes: (a) a proper coordination number and the chemical nature of ligands, ⁶¹ (b) a flexible coordination sphere, ^{62,63} and (c) inclusion of noncovalent interactions of the second coordination shell residues. ^{64,65} Most importantly, all these factors need to be synchronized to facilitate optimal binding and activation of substrates, stabilization of transition states, and departure of the leaving groups. However, it is not

Received: November 23, 2022 Revised: January 19, 2023 Published: February 16, 2023





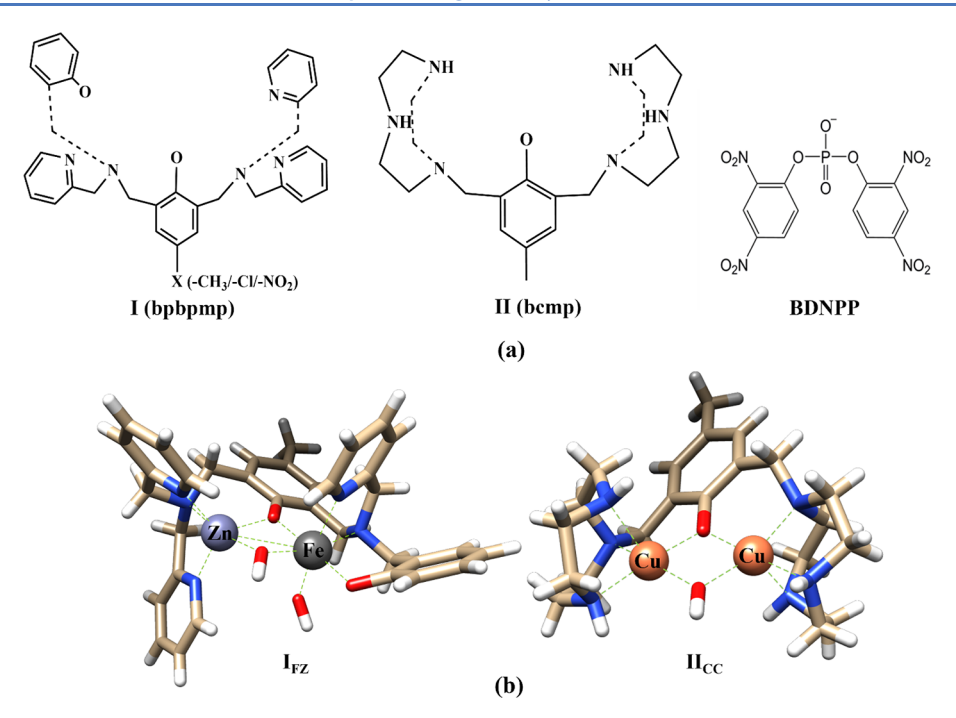


Figure 1. (a) Structures of the I and II ligands and BDNPP substrate. (b) Crystal structures of I_{FZ} and II_{CC} complexes.

trivial to separate and elucidate the influence of these factors experimentally. $^{55,66-71}$

In this study, on the basis of experimental data, these effects have been investigated in a systematic manner for a variety of binuclear metal complexes and their ability to hydrolyze phosphoester bonds. This is one of the most fundamental reactions in nature and ubiquitous in a wide range of critical biological, biotechnological, and agricultural processes. In biology, it is associated with signal transduction, DNA repair, RNA maturation, energy metabolism, and regulation of phosphate levels of plants, fungi, and mammals. I,62,72-77 biotechnology, it has been implicated in genomics, 78 therapeutics, 79,80 as well as the remediation and/or inactivation of highly toxic compounds such as pesticides and nerve agents (including sarin and tabun). 6,20,73,81-85 Specifically, in agriculture, the catalyst-promoted hydrolysis of phosphoester bonds is an attractive strategy for soil decontamination caused by the excessive use of pesticides such as malathion, parathion, and diazinon to increase crop production. 6,82,86,87 There have been intensive efforts to design a variety of metal complexes with distinct metal ions (transition and lanthanide) and ligand environments (symmetric and asymmetric) to hydrolyze phosphoester bonds under nondenaturing pH and temperature conditions. 28,62,88-90 In these reactions, the metal ions, generally Zn^{II}, Fe^{II/III}, Mn^{II}, Cu^{II}, Ca^{II}, and Mg^{II}, play multiple roles such as substrate activation, nucleophile generation, and stabilization of the transition states, intermediates, and leaving groups. 23,62,76,91 Because of the high Lewis acidity and low ligand field stabilization energy of the metal ions required in these reactions, both $Cu^{II3,92-95}$ and $Zn^{II28,66,96-111}$ have been extensively utilized. Additionally, Zn is redox inactive and the most abundant biological metal ion in natural metallohydrolases. 112-116 On the other hand, in the absence of any redox chemistry required for these reactions, the use of Fe, Mn, and Cu ions is quite intriguing.

Neves and co-workers synthesized the first heterobinuclear asymmetric Fe^{III} - Zn^{II} core-containing complex, $[I(OH)Fe^{III}(\mu$ -

 $OH)Zn^{II}$]⁺ (I_{FZ} , where I (bpbpmp) = 2-bis[{(2-pyridylmethyl)-aminomethyl}-6-{(2-hydroxybenzyl)-(2-pydidylmethyl)}aminomethyl]-4-methylphenol), that contains catalytically active $[(OH)Fe^{III}(\mu - OH)Zn^{II}(OH_2)]^+$ species in an aqueous solution (Figure 1). 117 In I_{FZ} , Fe^{III} is coordinated to the N_2O_2 site of the ligand I, whereas Zn^{II} is bound to the N₃O site. This complex mimics the structural and functional properties of purple acid phosphatases (PAPs) and accelerates the turnover rate for the hydrolysis of bis(2,4-dinitrophenyl) phosphate (BDNPP) by 4.8×10^3 -fold ($k_{\text{cat}} = 9.13 \times 10^{-4} \text{ s}^{-1}$) at pH 6.5. The measured kinetic isotope effect of $k_{\rm H}/k_{\rm D}$ = 1.34 suggests an intramolecular attack by the Fe^{III}-bound hydroxide in the rate-limiting step, 117 whereas the spectral change in the reaction mixture at pH 6.5 in the presence of excess substrate indicates that BDNPP binds directly to the ZnII ion. In contrast, Erxleben and co-workers reported a homobinuclear Cu^{II} - Cu^{II} core-possessing symmetric complex, [IICu^{II}(μ -OH)- Cu^{II}]²⁺ (II_{CC}), where II (bcmp) = 2,6-bis(1,4,7-triazacyclonon-1-ylmethyl)-4-methylphenol), that hydrolyzes BDNPP (Figure 1)^{17,118} with a second-order rate constant of 0.047 M^{-1} s⁻¹ at pH 8.0 and 40 °C. II_{CC} is also able to hydrolyze DNA and induce cell death in pancreatic cancer cells. In this complex, both Cu ions are coordinated to the symmetric N₃O ligands in II. The measured $k_{\rm H}/k_{\rm D}$ effects for II_{CC} suggest that a bridging hydroxyl group, unlike the terminal water molecule in I_{FZ}, acts as the nucleophile in the reaction. 118 Its Zncontaining variant (II_{ZZ}) also hydrolyzes BDNPP with an apparent second-order rate constant of 0.028 M⁻¹ s⁻¹ under the same conditions. 103 The dependence of the hydrolysis rate on the concentration of these metal complexes suggests a weak binding of BDNPP to II_{CC} and II_{ZZ}.

Phosphoester hydrolysis by metal complexes of ligands I and II can occur through a mechanism that may employ any of the four pathways shown in Scheme 1:^{39,119–121} (1) dissociative (DA), (2) substrate-assisted (SA), (3) water-assisted (WA), and (4) associative (AS). As discussed above, they can utilize either the terminal or bridging hydroxyl group as a nucleophile.

Scheme 1. Proposed Reaction Pathways for Phosphodiester Hydrolysis

However, only the terminal hydroxyl is used in the pathways depicted in Scheme 1. According to the DA pathway, 12 the metal ion-bound hydroxyl nucleophile attacks the substrate and cleaves the scissile P-Ot bond in an S_N2 fashion. In this mechanism, backside attack of the nucleophile on the electrophile is favorable as it inverses the conformation of the product, and this inversion minimizes the repulsion between lone pair electrons on the leaving group and the nucleophile. In the SA pathway, 125-127 unlike the previous DA pathway, the hydroxyl nucleophile is split; i.e., the proton is transferred to the oxygen atom (O5) of the phosphate group, whereas the oxygen (O1) attacks the electrophilic P atom of the substrate BDNPP to cleave the P-Ot bond. In the WA pathway, 128,129 the metal bound hydroxyl group (-O¹H¹) functions as a base and abstracts a proton (H3) from an external water to create the hydroxyl (-OWH) nucleophile. This group simultaneously attacks the P atom and cleaves the phosphoester bond. In the AS pathway, ^{66,130,131} the cleavage of the scissile phosphoester bond (P-Ot) takes place through the formation of the phosphorane intermediate in a stepwise

In these four pathways, many fundamental chemical properties such as the catalyst-substrate complexation and electronic nature of the metal ion, ligand environment, linker, and nucleophile play key roles. 132 Additionally, the Lewis acidity of the metal ion and nucleophilicity of hydroxyl ion can be critical. 34,133,134 Furthermore, the BDNPP substrate can bind in either a monodentate or bidentate manner to achieve either Lewis or double Lewis activation, respectively. The metal cooperativity is also important in the functioning of the binuclear metal complexes. ^{105,135,136} Furthermore, the *para*substitution of the bridging phenolic oxygen of the linker has been reported to influence the rate of hydrolysis (Figure 1). 100 The nature of the nucleophile (bridging -OH, terminal -OH, or -O₂H₃) also affects the rate of the reaction. ^{137,138} Finally, the introduction of an external electric field along the reaction axis, the direction along which electrons reorganize, has been reported to affect the structures and reactivities of complexes. 139-141 Whereas an orientation of the electric field parallel to the reaction axis can accelerate a reaction, an antiparallel alignment may have the opposite effect.

In this study, on the basis of experimental data, all these chemical factors have been systematically investigated using two chemically distinct ligands (asymmetric (I)) with three different (hetero- and homobinuclear) metal

ion combinations (i.e., Fe^{III} - Zn^{II} , Zn^{II} - Zn^{II} , and Cu^{II} - Cu^{II}) of I (I_{FZ}, I_{ZZ}, and I_{CC}) and II (II_{FZ}, II_{ZZ}, and II_{CC}); BDNPP, an analogue of DNA, is used as model substrate (Figure 1). Additionally, three different nucleophiles (μ -OH, terminal-OH, and $-O_2H_3$) and para substituents (-CH₃, -Cl, and -NO₂) of the linker have been utilized. The effects of coordination number and charge of metal ions on the energetics are also studied by altering the number of hydroxyl groups. Furthermore, the influence of an external electric field on the activities of these complexes is investigated. The combined results from our study will provide a deeper understanding of the roles of these distinct fundamental chemical factors in one of the most critical reactions in nature. They may also help us derive principles for the design of the next generation of synthetic analogues to catalyze the hydrolysis of phosphates, peptides, and nitriles and other reactions including epoxide opening, aldol condensation, Michael addition, and Diels-Alder reactions. 61,142–151

2. COMPUTATIONAL DETAILS

The structures of metal complexes of the I $(I_{ZZ}$ and $I_{CC})$ and II (II_{FZ}) ligands were built using the X-ray structures of I_{FZ} , II_{CC} , and II_{ZZ} 118 (Figure 1b). As discussed below, multiple spin states and BDNPP substrate binding modes were explored to determine their ground states. All calculations were performed using the Gaussian 09 program package. 152 The geometries of reactants, transition states, intermediates, and products were optimized without any symmetry constraints at the mPW1PW91¹⁵³/LANL2TZ (+)¹⁵⁴ level of theory utilizing the Hay-Wadt effective core potential 155 for metal atoms. The 6-311+G(d) basis set was used to treat the P atom; 6-31+G(d) basis set for the N and O atoms; and 6-31G(d) for the C, H, and Cl atoms. This DFT functional has been reported to provide accurate structural and electronic properties of metal complexes. 156,157 Hessians were calculated at the same level of theory as optimizations to confirm the nature of the stationary points along the reaction coordinates. Furthermore, internal redundant coordinate (IRC)¹⁵⁸ calculations were performed to confirm the connection between the corresponding transition states and minima. Grimme D3 dispersion corrections were also incorporated in the optimizations. 159 Additionally, solvent effects were calculated using diethylether (dielectric constant, ε = 3.1) using the self-consistent reaction field-SMD implicit solvent model (SCRF-SMD). The kinetic data for I_{FZ} , II_{ZZ} , and II_{CC} were collected in a buffer solution. Because it is not possible to simulate experimentally used buffer using dielectric constants and these complexes are supposed to be enzyme mimics, diethylether was used to simulate the hydrophobic environment of an enzyme active site. It is noteworthy that these solvent effects are not very sensitive on the value of the dielectric constant for structures with the same charge. 161 Furthermore, natural bonding orbital (NBO) charges for all optimized structures were computed. 162 The final energies of the optimized structures were further improved by performing single point calculations using the triple- ζ basis set 6-311+G(d+p). Zero-point vibrational (unscaled), thermal (at 298.15 K and 1 atm), solvent, and entropy corrections (at 298.15 K) were added to the final energies of the optimized structures. To assess the effects of the DFT functional on computed energetics, the DA pathway was investigated using the B3LYP, 163 M06L, 164 and M06-2X¹⁶⁵ functionals. The B3LYP and M06L functionals were found to increase the barrier by 1.8-2.9 kcal/mol, whereas the

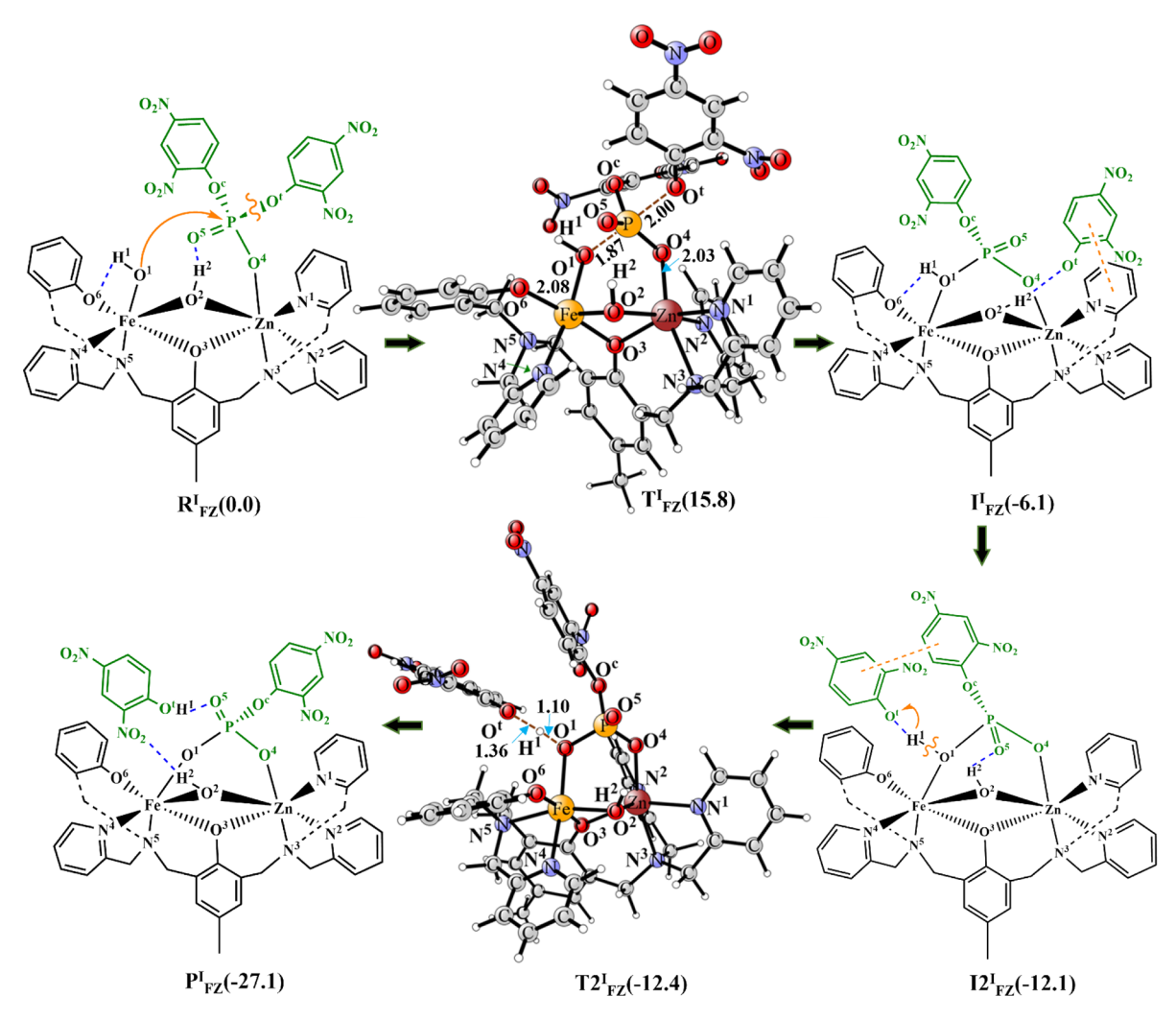


Figure 2. Optimized structures for I_{FZ} in the DA pathway.

M06-2X functional lowered the barrier by 1.6 kcal/mol. The effect of external electric fields was investigated using the keywords "Field = $M \pm N$ " that define the axis of the electric field (direction and magnitude). Initially, a range of field strengths (F = -0.05 to +0.05 au, 1 au = 51.4 V Å⁻¹) were introduced along all the X, Y, and Z axes. On the basis of these calculations, the Field = Z + 10 (along the Z axis, +0.01 au) was selected. All these structures were subsequently optimized using Field = Z + 10 at the same level of theory as used for geometry optimizations.

3. RESULTS AND DISCUSSION

In this study, hydrolytic activities of six distinct complexes that include three metal ion combinations for ligands I (I_{FZ} , I_{ZZ} , and I_{CC}) and II (II_{FZ} , II_{ZZ} , and II_{CC}) are investigated using four diverse pathways (DA, SA, WA, and AS; Scheme 1). Their energetics is compared in terms of Lewis acidity, nucleophilicity, basicity, and metal cooperativity using the metal—substrate, metal—nucleophile, metal—ligand, and metal—metal distances and atomic charges (NBO) as parameters. ^{133,134} Additionally, natural bond analysis of the optimized structures is performed to rationalize their reactivities.

3.1. Structures of Metal Complexes. On the basis of their metal and ligand compositions, complexes of I (I_{FZ} , I_{ZZ} , and I_{CC}) and II (II_{FZ} , II_{ZZ} , and II_{CC}) adopt different

geometries and spin states. Both IFZ and IIFZ can exist in three different spin states (doublet, quartet, and sextet). I_{FZ} exists in a high-spin sextet ground state, whereas the doublet and quartet states are 12.2 and 15.6 kcal/mol, respectively, higher in energy in the gas phase (Figure S1). II_{FZ} showed the same pattern; i.e., the doublet and quartet spin states are 11.2 and 15.9 kcal/mol, respectively, less favorable than the sextet ground state (Figure S2). In the sextet state of I_{E7} , the terminal hydroxyl group is coordinated to the Fe^{III} ion in the N₂O₂ site, similar to the X-ray structure of IFZ, whereas it is bridging in the other two spin states. The $\mathrm{Zn^{II}} ext{-}\mathrm{Zn^{II}}$ core-containing I_{ZZ} and II_{ZZ} complexes exist only in the singlet state and two different conformations, i.e., a terminal (Zn1-OH) and a bridging $(\mu$ -OH) or $(\mu$ -OH)₂ (Figure S3). The optimization of the Zn2-OH conformation of Izz also converged to the bridging $(\mu\text{-OH})_2$ structure. On the other hand, the Cu^{II}-Cu^{II} core in complexes I_{CC} and II_{CC} can exist in the broken symmetry singlet and triplet spin states. For I_{CC}, both these states are degenerate, and the optimized structures adopt the same geometry, i.e., one bridging and one Cu2-bound terminal hydroxyl group (Figure S4). On the other hand, for II_{CC}, the triplet state is slightly lower in energy (by 0.8 kcal/mol) than the open shell singlet state. In the triplet state, both hydroxyl groups are terminally coordinated, whereas in the broken symmetry singlet state, one is terminal and the other one is

Table 1. Key Bond Distances (Å) of the Optimized Structures for IFZ, IZZ, and ICC in the DA and SA Pathways

I	$R^{I}_{\ FZ}$	$R^{I}_{\ ZZ}$	R^{I}_{CC}	$T^I_{\ FZ}$	$T^I_{\ ZZ}$	T^{I}_{CC}	$T^{I'}_{FZ}$	$T^{I'}_{\ ZZ}$	$T^{I'}_{CC}$	$T1_{FZ}^{SA}$	$T1_{ZZ}^{SA}$	$T1_{CC}^{SA}$
M_1 - O^1	1.89	2.10	3.98	2.08	3.88	3.90	2.14	3.80	3.56	1.99	3.69	3.99
M_1 - O^2	1.97	2.11	1.94	1.94	2.07	2.04	1.92	2.06	2.31	1.97	2.09	1.98
M_1 - O^3	2.11	2.19	1.97	2.00	2.12	1.96	2.00	2.14	1.99	2.02	2.10	1.95
M_1 -O ⁴	4.78	4.49	4.34	3.55	2.22	2.39	3.51	2.20	2.07	3.54	2.14	2.85
M_1 - N^4	2.27	2.33	2.28	2.34	2.31	2.16	2.33	2.38	2.14	2.22	2.31	2.13
M_1 - N^5	2.26	2.25	2.16	2.19	2.28	2.31	2.17	2.27	2.37	2.29	2.38	2.36
M_1 -O ⁶	1.93	2.02	1.94	1.89	2.00	1.92	1.89	2.02	1.92	1.88	2.00	1.92
M_2 - O^1	3.66	2.04	1.88	3.30	2.12	2.14	3.29	2.15	2.11	3.30	2.04	2.00
M_2 - O^2	2.04	2.08	1.98	2.17	2.03	1.92	2.20	2.01	1.91	2.16	2.06	1.95
M_2 - O^3	2.13	2.09	2.35	2.10	2.07	2.02	2.09	2.06	2.04	2.06	2.06	2.06
M_2 -O ⁴	2.12	4.28	3.95	2.03	2.78	2.75	2.00	3.12	3.18	2.03	3.20	2.84
M_2 - N^1	2.26	2.23	2.08	2.15	2.26	2.27	2.38	2.22	2.23	2.35	2.27	2.40
M_2 - N^2	2.23	2.27	2.39	2.24	2.29	2.08	2.16	2.30	2.09	2.15	2.30	2.09
M_2 - N^3	2.28	2.49	2.22	2.36	2.52	2.62	2.24	2.40	2.40	2.26	2.40	2.75
O¹-P	5.32	3.96	4.40	1.87	1.88	1.79	1.76	1.76	1.78	1.76	1.76	1.73
P-O ^t	1.67	1.68	1.70	2.00	2.03	2.18	1.71	1.79	1.82	1.90	1.84	1.90
P-O ^C	1.66	1.69	1.69	1.67	1.72	1.72	2.12	2.07	1.93	1.67	1.71	1.72
O^1 - H^1	0.97	0.97	0.96	0.97	0.97	0.97	0.98	0.97	0.98	1.23	1.22	1.24
H^1 - O^C	6.21	4.46	3.87	2.51	2.13	2.13	1.91	1.80	1.82	2.74	2.87	2.88
H1-O5	4.92	3.74	4.78	2.54	3.19	3.08	2.74	3.18	3.01	1.26	1.25	1.23
M_1 - M_2	3.13	2.74	3.16	3.08	2.98	2.88	3.08	3.02	3.03	3.08	3.04	2.88

bridging (Figure S5). In I_{CC} , the terminal hydroxyl group, equivalent to the Fe^{III}-bound hydroxyl group in I_{FZ} , can be coordinated to either Cu1 or Cu2. However, the structure with the Cu2-bound hydroxyl is 8.1 kcal/mol lower in energy than its Cu1-coordinated counterpart in the triplet ground state (Figure S4). The metal—ligand distances in the optimized structures of I_{FZ} , II_{CC} , and II_{ZZ} are in good agreement with their corresponding X-ray structures (Table S1).

3.2. Substrate Binding. The substrate BDNPP can interact with the metal centers either in a monodentate (to either M1 or M2) or bidentate (both M1 and M2) manner or indirectly *via* hydrogen bonding. After extensive conformational sampling of these complexes, the energetically most stable structures were used to investigate their mechanisms (Figures S6–S8). The substrate binding mode is found to be influenced by the nature of the metal ion and ligand environment. For instance, in I_{FZ}, it binds directly to the Zn ion, whereas it interacts only through hydrogen bonding in II_{FZ} (Figure S6). It also associates in an indirect manner in the I_{ZZ}, II_{ZZ}, I_{CC}, and II_{CC} complexes (Figures S7 and S8). The binding mode of I_{FZ} is also supported by experimental data. ¹¹⁷ The catalyst–substrate interactions are discussed in detail below.

3.3. Mechanisms of Phosphodiester Hydrolysis. On the basis of the available experimental and theoretical data, the hydrolysis of BDNPP by the different metal ion combinations of I (I_{FZ} , I_{CC} , and I_{ZZ}) and II (II_{FZ} , II_{CC} , and II_{ZZ}) is investigated using the four reaction pathways illustrated in Scheme 1.

3.3.1. Dissociative (DA) Mechanism. In the reactant (R_{FZ}^{I}) of I_{FZ} , both Fe^{III} and Zn^{II} ions have six ligands in a distorted octahedral coordination environment (Figure 2). Fe^{III} is located in the N_2O_2 site and Zn^{II} is in the N_3O site of the asymmetric ligand I. A terminal hydroxyl ($-O^1H^1$) is also bound to the Fe^{III} atom, and a second hydroxyl group ($-O^2H^2$) and the p-methylphenolate group of the ligand I bridge the two metal ions. The Fe^{III} - Zn^{II} distance is 3.13 Å (Table 1). This distance is 0.43 Å shorter than the one in the Fe^{III} - Zn^{II} core of

the enzyme glycerophosphodiesterase (GpdQ). 166,167 BDNPP is coordinated to the ZnII ion in a monodentate fashion through its most electronegative oxygen (O4, -0.57e) atom $(Zn^{II}-O^4 = 2.12 \text{ Å}, Figure 2)$. This substrate binding mode is in line with experimental data reported for I_{FZ}. 117 However, rather surprisingly, no Lewis acid activation of the substrate is observed in RIFZ, and the catalyst-substrate interaction actually strengthens the scissile P-Ot bond by 0.04 Å in comparison to the corresponding bond in its free form. This is in contrast to the activation of the scissile P-O bond of BNPP in the mechanisms employed by GpdQ¹⁶⁶ or the Zn^{II}-Zn^{II} core-containing Streptomyces griseus aminopeptidase (SgAP)¹⁶⁸ enzymes. In RIF7, BDNPP binding is further stabilized through hydrogen bonding with the bridging $-O^2H^2$ group (H^2-O^5) 2.16 Å). In this structure, the highest occupied molecular orbital (HOMO) is localized on the Fe^{III} site (Figure S9). On the other hand, the lowest unoccupied molecular orbital (LUMO) and LUMO+1 are localized on the substrate, with the LUMO being predominantly on its leaving group (Figure S9). In an S_N2-type reaction, an in-line concerted attack of the Fe^{III} bound -O¹H¹ nucleophile on the electrophilic P atom of BDNPP leads to the cleavage of the scissile P-Ot bond with a barrier of 15.8 kcal/mol. It is in good agreement with the measured barrier of 20.1 kcal/mol. 117 This barrier is, however, 5.7 kcal/mol higher than the corresponding barrier computed for GpdQ, 166 demonstrating that RIFZ, formed by organic ligands, is substantially less active than biological hydrolases created by amino acid residues. The optimized transition state (T_{FZ} in Figure 2) is stabilized by the formation of two additional hydrogen bonds between the catalyst and substrate in comparison to RIFZ. In TIFZ, the Fe-Zn distance shrinks by 0.05 Å, and the Fe-O¹H¹ nucleophile bond weakens by 0.19 Å. As a result, the charge on the O2 atom of the bridging hydroxyl (-O²H²) reduces by 0.05e and the charge on the O¹ atom of the nucleophile increases by 0.7e in the $R^{I}_{FZ} \rightarrow T^{I}_{FZ}$ transformation. However, the charges on both metals remain unchanged. During the nucleophilic attack, the LUMO of R¹_{FZ} gets populated and stabilized to become HOMO-1 of T_{FZ}

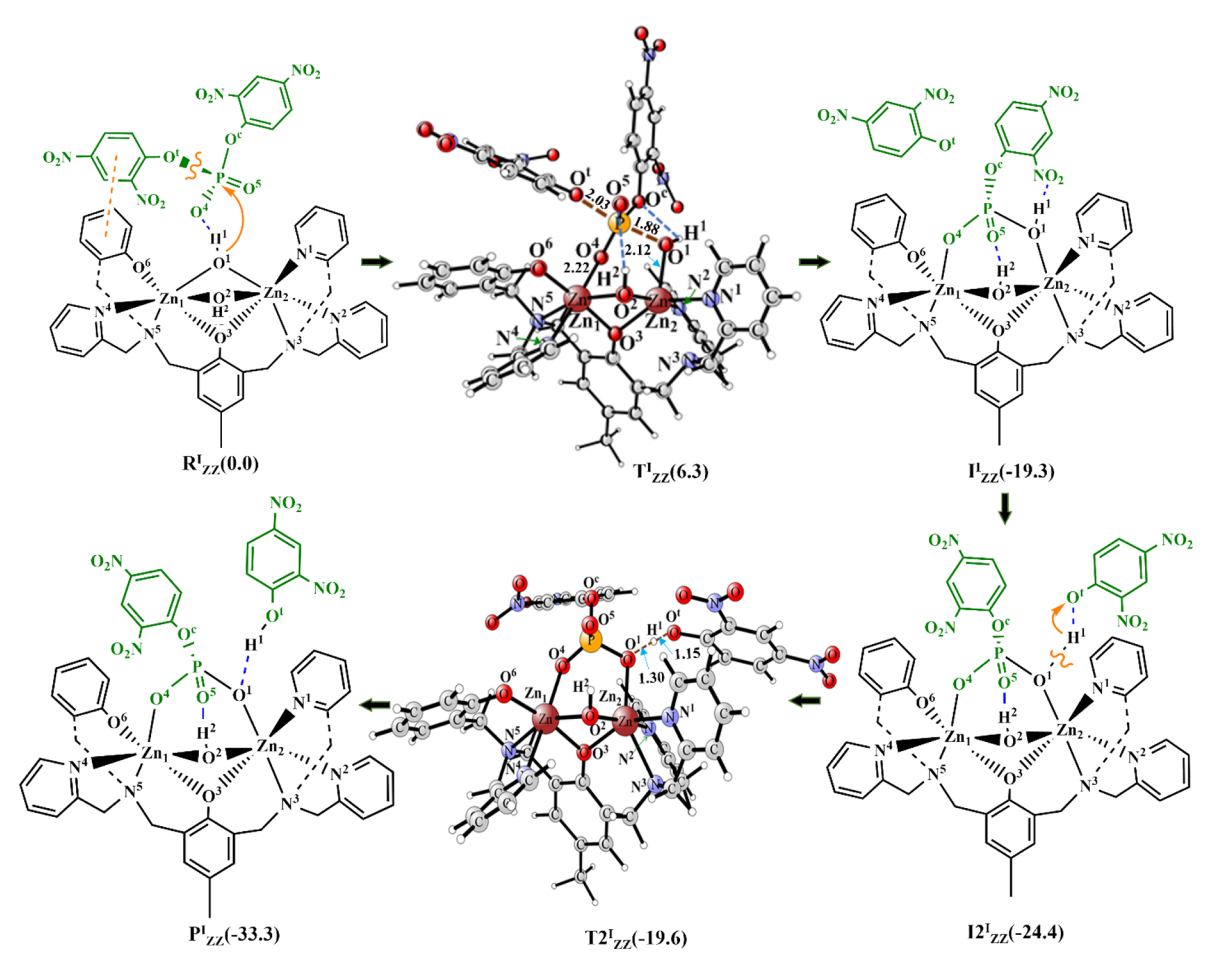


Figure 3. Optimized structures for IZZ in the DA pathway.

(Figure S9). Therefore, a lower HOMO-LUMO gap is expected to promote the population of the LUMO of R_{FZ}^{I} during the reaction (the HOMO-LUMO energy gap for this complex is 0.1022 hartree). The P-O¹ and P-O^t bond lengths in T_{FZ}^{I} confirm the concerted nature of this process (P-O¹ = 1.87 Å and P-O^t = 2.00 Å). In contrast to the use of double Lewis acid activation by the binuclear metal cores of natural hydrolases, this mechanism is dominated by the nucleophilicity of the Fe^{III}-coordinated -O¹H¹ group. The negatively charged dinitrophenolate group released in this process is a good leaving group and forms the product (I_{FZ}^{l}) that is exergonic by 6.1 kcal/mol. However, the monoester group in I_{FZ}^{I} is still bound to the metal complex. The 2,4-dinitrophenolate group can be easily neutralized through the abstraction of the H¹ proton from the -O¹H¹ group. This process occurs through the formation of another intermediate (I2^I_{FZ}) that is 6.0 kcal/mol more exergonic than II_{FZ}. From I2I_{FZ}, an almost barrierless proton transfer through the transition state (T2^I_{FZ}) generates a neutral product (PIFZ) that is 27.1 kcal/mol more exergonic than RIFZ.

In contrast to R^{I}_{FZ} , BDNPP in dizinc core-containing R^{I}_{ZZ} does not coordinate directly to the metal ions. In this structure, both hydroxyl groups (μ -O¹H¹ and μ -O²H²) bridge the two Zn^{II} ions, and thus, there is no vacant coordination site for the substrate (Figure 3). However, the substrate interacts through a strong hydrogen bond with the μ -O¹H¹ group and π - π interactions with the 2-hydroxybenzyl group of the ligand of Zn1 (Figure 3). In R^{I}_{ZZ} , the metal-metal distance is shorter

and the metal-ligand bonds are longer than the corresponding distances in R_{FZ}^{I} (Table 1). From R_{ZZ}^{I} , the computed barrier for the cleavage of the P-Ot bond through the attack by the -O¹H¹ nucleophile is only 6.3 kcal/mol, which is 9.5 kcal/mol lower than the barrier in IFZ. This is surprising because a hydroxyl group bound to two metal ions should be a weaker nucleophile than one bound to only one metal ion. However, because of the low ligand field stabilization energy of the Zn ion, both metal-nucleophile distances (Zn_1 -O¹ = 2.10 Å and Zn_2 -O¹ = 2.04 Å) in R^I_{ZZ} are substantially longer than the FeO¹ distance in R^I_{FZ} (1.89 Å; Table 1). The nucleophile $(-O^1H^1)$ -electrophile (P) distance in R^I_{ZZ} (O^1 -P = 3.96 Å) is also much shorter than the one in R_{FZ}^{I} (O¹-P = 5.32 Å). Additionally, in the transition state (T^{I}_{ZZ}) , the substrate is coordinated to the Zn1 center, and the μ -O¹H¹ nucleophile becomes terminal (Figure 3). Interestingly, in T^{I}_{ZZ} , the -O¹H¹ nucleophile is bound to the metal in site 2 (Zn₂), contrasting the situation in the reaction with R^I_{FZ} , where the nucleophile is located at site 1 (Fe1). In the $R^I_{ZZ} \rightarrow T^I_{ZZ}$ process, in contrast to R^I_{FZ} , the charge on the O^2 atom of the bridging hydroxyl (-O²H²) increases by 0.03e, and the charge on the O¹ atom of the nucleophile decreases significantly by 0.18e. Furthermore, the charge on only Zn1 increases by 0.03e, whereas the charges on both metals remain intact in RIFZ. The Zn-Zn distance also follows the opposite trend and increases by 0.24 Å (Table 1). Hence, in summary, the reason for the significantly lower barrier in R^{I}_{ZZ} when compared to R^{I}_{FZ} is the provision of a stronger nucleophile in the former.

Figure 4. Optimized structures for I_{CC} in the DA pathway.

Similar to R^{I}_{ZZ} BDNPP does not bind directly to the metal ions in the dicopper core-possessing R¹_{CC} (coordination numbers are 5 and 6 for Cu1 and Cu2, respectively). However, the substrate binding mode is quite different in the two systems. In RI_{CC}, the substrate associates through hydrogen bonding with the single bridging hydroxyl (μ -O²H²) and via π - π interactions with the 2-pyridylmethyl group of the ligand of the Cu2 site (Figure 4). In this structure, the -O¹H¹ group is terminally bound to the Cu2 atom (Figure 4 and Table 1). The Cu1-Cu2 distance (3.16 Å) is longer than the metal-metal distances in RIFZ and RIZZ. The metal-nucleophile bond (Cu2- $O^1 = 1.88 \text{ Å}$) in $\mathbf{R}^{\mathbf{I}}_{CC}$ is comparable to that in $\mathbf{R}^{\mathbf{I}}_{FZ}$ (1.89 Å). Despite the lack of a direct bond between the metal and substrate, the P-O t bond in R^{I}_{CC} is 0.03 Å more activated than that in in \mathbf{R}_{FZ}^{I} (P-O^t = 1.70 Å). The nucleophile (-O¹H¹)—electrophile (P) distance in \mathbf{R}_{CC}^{I} (O¹-P = 4.40) is shorter than that in R_{FZ}^{I} but longer than that in R_{ZZ}^{I} (Table 1). For R_{CC}^{I} , the barrier for the cleavage of the P-Ot bond is 11.4 kcal/mol, which is 4.4 kcal/mol lower and 5.1 kcal/mol higher than the corresponding barrier for IFZ and IZZ, respectively. Similar to T^{1}_{ZZ} , the nucleophile is provided by the Cu2 site in the transition state (TI_{CC}). The metal-metal distance in this system follows the same pattern as observed for IFZ; i.e., in TI_{CC}, the Cu-Cu distance decreases by 0.28 Å and the Cu2-O¹H¹ nucleophile bond elongates by 0.26 Å. Moreover, the charge on the O² atom of the bridging hydroxyl (-O²H²) gets lowered by 0.03e and the one on the O1 atom of the nucleophile increases by 0.3e in the $R^{I}_{CC} \rightarrow T^{I}_{CC}$ transformation. In this process, the charge on the nucleophile providing Cu2 increases by 0.03e. Similar to RIFZ, the HOMO of RICC is positioned on site 1 (Figure S10). Here, both the LUMO and LUMO+1 are on the substrate, with the LUMO again localized on its leaving group. In the $R^{I}_{CC} \rightarrow T^{I}_{CC}$ transition, the LUMO of RICC gets stabilized to become the HOMO-1 of T^I_{CC} (Figure S10). However, the HOMO-LUMO energy gap of 0.0861 hartree in this case is smaller than the corresponding gap of 0.1022 hartree for R_{FZ}^1 . This lower gap should make it easier to populate the LUMO of the reactant, which correlates well with the 4.4 kcal/mol lower barrier for RICC.

The cis bond (P-O c) of BDNPP is also accessible for cleavage through this mechanism (Figure 2). However, in comparison to the trans bond, the barrier for the splitting of this bond by I_{FZ} , I_{CC} , and I_{ZZ} through the DA mechanism is

higher by 9.2, 8.7, and 14.3 kcal/mol, respectively. The strain of the four-membered transition states ($\mathbf{T}^{I'}_{FZ}$, $\mathbf{T}^{I'}_{CC}$, and $\mathbf{T}^{I'}_{ZZ}$ in Figure S11) created in this process caused this increase in the barrier. Nonetheless, the reactivities of all three complexes for the cleavage of the *cis* and *trans* P-O bond follow exactly the same order, *i.e.*, $\mathbf{I}_{ZZ} > \mathbf{I}_{CC} > \mathbf{I}_{FZ}$.

The above results demonstrate that the ligand environments and substrate binding modes of the three distinct metal clusters for the same ligand differ significantly from each other. Additionally, key parameters such as metal—metal distances and charges follow a distinct pattern in these systems. Despite the lack of direct coordination to any of the metal ions, the scissile P-O¹ bond of BDNPP in both R^I_{ZZ} and R^I_{CC} is more activated than the corresponding bond in R^I_{FZ} (Table 1). Quite clearly, in the absence of a Lewis acid activation, the energetics of this process is dominated by the nucleophilicity of the hydroxyl ion.

3.3.2. Substrate-Assisted (SA) Mechanism. In this mechanism, the O1-H1 bond of the FeIII-bound O1H1 nucleophile of R_{FZ}^{I} is broken, and the O^{1} and H^{1} atoms are transferred to the P and O⁵ atoms of BDNPP, respectively (Figure S12). This process leads to the simultaneous cleavage of the P-Ot bond and the release of the negatively charged dinitrophenolate group through the transition state $(T1_{EZ}^{SA})$ (Figure S12). This concerted process occurs through the high barrier of 35.6 kcal/ mol because of the additional energy required for the cleavage of the $-O^1H^1$ bond. The intermediate (\mathbf{I}_{FZ}^{SA}) formed in this step is exergonic by 25.4 kcal/mol. Similarly high barriers of 29.2 and 28.9 kcal/mol for this step are also computed for the corresponding I_{CC} and I_{ZZ} complexes, respectively (Figures S13 and S14). Because this mechanism occurs with prohibitively high barriers for all three systems, it can be ruled out.

3.3.3. Water-Assisted (WA) Mechanism. In this mechanism, the Fe^{III}-bound -O¹H¹ group in the reactant (R_{FZ}^{IWA} in Figure S15a) functions as a base and abstracts the H³ proton from the outer sphere water (H³O^WH⁴) molecule to create the -O^WH⁴ nucleophile. The -O^WH⁴ group concomitantly attacks the electrophilic P atom and breaks the P-O^t bond of the substrate. All key bond distances in the transition state (T_{FZ}^{IWA}) of this process confirm its concerted nature (O¹-H³ = 1.19 Å, H³-O^W = 1.22 Å, O^W-P = 1.97 Å, and P-O^t = 1.84 Å in Table 2). The barrier of 22.6 kcal/mol for this mechanism is 6.8 kcal/mol higher than the barrier (15.8 kcal/mol) computed for the

Table 2. Key Bond Distances (Å) of the Optimized Structures for I_{FZ} , I_{ZZ} , and I_{CC} in the WA Pathway

I	$R_{FZ}^{IWA} \\$	$R_{ZZ}^{IWA} \\$	R_{CC}^{IWA}	T_{FZ}^{IWA}	$T_{ZZ}^{IWA} \\$	T_{CC}^{IWA}
M_1 - O^1	1.91	4.05	3.88	2.02	4.10	3.97
M_1 - O^2	1.98	2.03	1.95	1.94	2.04	1.98
M_1 - O^3	2.03	2.14	1.97	2.01	2.12	2.00
M_1 - O^4	3.97	2.22	4.38	3.90	2.25	3.27
M_1 - N^4	2.28	2.26	2.16	2.21	2.31	2.27
M_1-N^5	2.25	2.35	2.26	1.92	2.28	2.19
M_1 - O^6	1.93	2.04	1.94	2.32	2.01	1.92
M_2 - O^1	3.39	2.00	1.89	3.62	2.04	1.95
M_2 - O^2	2.04	2.03	1.96	2.15	2.03	1.92
M_2 - O^3	2.18	2.14	2.30	2.12	2.16	2.27
M_2 - O^4	2.16	3.47	4.03	2.04	3.23	3.87
M_2 - N^1	2.23	2.32	2.45	2.22	2.33	2.52
M_2 - N^2	2.18	2.30	2.09	2.25	2.26	2.07
M_2 - N^3	2.40	2.59	2.21	2.39	2.56	2.17
O^1 - H^3	1.80	1.67	1.60	1.19	1.38	1.21
H^3 - O^W	0.98	1.00	1.01	1.22	1.09	1.22
O^W -P	3.81	2.86	5.62	1.97	2.05	2.04
P-O ^t	1.68	1.68	1.69	1.84	1.88	1.87
P-O ^C	1.65	1.67	1.69	1.69	1.72	1.71
M ₁ -M ₂	3.09	3.10	3.12	3.18	3.10	3.06

corresponding DA mechanism. In the product (P_{FZ}^{IWA}) , the monoester group (DNPP) is coordinated to the Zn ion, and it is 6.0 kcal/mol exergonic from $R_{\rm FZ}^{\rm IWA}$. In comparison to the heterobinuclear R_{FZ}^{IWA} , in the homobinuclear reactants R_{ZZ}^{IWA} and \mathbf{R}_{CC}^{IWA} , the -O¹H¹ base is bound to the metal ion in site 2. In R_{ZZ}, BDNPP is directly coordinated to the Zn1 ion, whereas in R_{CC}, it is hydrogen bonded to a Cu2-coordinated water and μ -O²H² (Figure S15b,c). The barrier for this mechanism is 14.3 and 24.2 kcal/mol for Izz and Icc, respectively, i.e., 8.0 and 12.8 kcal/mol higher than the corresponding barriers in the DA mechanism for I_{ZZ} and I_{CC}. Similar to the DA mechanism, however, the barrier for this mechanism is lowest for I_{ZZ} (14.3 kcal/mol), and the corresponding barriers for I_{FZ} and I_{CC} are substantially higher (i.e., 22.6 and 24.2 kcal/mol, respectively). That is likely to be due to the stronger basicity of the Zn_2 -O¹H¹ group in R_{ZZ}^{IWA} among the three complexes, linked to the longer metal-O¹ distance [2.00 Å (R_{ZZ}^{IWA}), 1.91 Å (R_{FZ}^{IWA}) , and 1.89 Å (R_{CC}^{IWA})] and higher charge on the O¹ atom $[-1.29e (R_{ZZ}^{IWA}), -0.51e (R_{CC}^{IWA}), \text{ and } -0.42e (R_{FZ}^{IWA})].$ These results demonstrate that this mechanism is energetically also less favorable than the DA mechanism. Among the three complexes, I_{ZZ} is, however, the most active complex in both DA and WA mechanisms.

3.3.4. Associative (AS) Mechanism. On the basis of the higher activity of I_{ZZ} in the previous mechanisms, the AS mechanism was investigated only for this complex (Figure S16). In the first step, from R^{IA}_{ZZ} , the Zn_2 bound hydroxyl ($\cdot O^1H^1$) group performs a nucleophilic attack on the electrophilic P atom of the substrate. This attack occurs through the transition state ($T1^{IA}_{ZZ}$) with a barrier of 13.1 kcal/mol. In $T1^{IA}_{ZZ}$, BDNPP is coordinated to the Zn^{II} ion in site 1 through the Zn^{II} bond. Here, the nucleophile–electrophile (O^1 -P) distance is decreased by 1.70 Å and the metal–nucleophile (Zn_2 - O^1) bond is shortened by 0.02 Å in comparison to R^{IA}_{ZZ} (O^1 -P = 2.26 Å and Zn_2 - O^1 = 2.02 Å). The nucleophilic attack in this step leads to the formation of the phosphorane intermediate (I^{IA}_{ZZ}), in which the substrate adopts a trigonal bipyramidal conformation around the P

center. In I^{IA}_{ZZ} , the P-O^t bond is activated significantly by 0.26 Å, and it is endergonic by 8.4 kcal/mol compared to R^{IA}_{ZZ} . The collapse of I^{IA}_{ZZ} leads to the release of the dinitrophenolate group of BDNPP in the product (P^{IA}_{ZZ}). P^{IA}_{ZZ} is exergonic by 10.7 kcal/mol compared to R^{IA}_{ZZ} , and the leaving group is stabilized by a hydrogen bond with the bridging hydroxyl group (-O²H²) and π – π stacking with the metal bound 2,4-dinitrophenyl phosphate fragment of the substrate.

In summary, AS is a plausible pathway among the four mechanistic pathways. However, the barrier (13.1 kcal/mol) for this mechanism is substantially higher (by 6.8 kcal/mol) than the one computed for the DA mechanism (6.3 kcal/mol) but is slightly lower (by 1.2 kcal/mol) than that of the WA mechanism (14.3 kcal/mol).

3.4. Ligand Effect. The effects of the symmetric (N_3-N_3) ligand II (Figure 1) on the energetics of the previous pathways for all three variants $(II_{FZ}, II_{CC}, and II_{ZZ})$ were also investigated. In the reactants for the DA pathway (RII FZ) RII and RII CC), BDNPP does not coordinate directly to the metal ions; rather, it interacts with the metal complex through multiple hydrogen bonds (only in R_{FZ}^{I} is the substrate directly coordinated to the Zn₂ ion; Figure 2). In R^{II}_{FZ}, in comparison to R¹_{FZ}, the metal-metal and all the metal-ligand distances are shorter (Table S2). Additionally, both metal-nucleophile $(Fe^{III}-O^1)$ and the scissile bond $(P-O^t)$ in R^{II}_{FZ} are shorter by 0.05 and 0.01 Å, respectively, than in R^{I}_{FZ} , suggesting the provision of a weaker nucleophile and stronger phosphoester bond in the former. However, the charges on the O² atom of the bridging hydroxyl (-O²H²) and the O¹ atom of the nucleophile follow a similar trend in both cases, i.e., decreases and increases for O^2 and O^1 , respectively, in the $R^{II}_{\ FZ} \rightarrow T^{II}_{\ FZ}$ process. In RII, the HOMO is located on the bridging phenolate linker (Figure S17). The LUMO and LUMO+1 are again positioned on the substrate, with the LUMO being localized predominantly on its leaving group. The LUMO of R^{II}_{FZ} gets populated and stabilizes to the HOMO of T^{II}_{FZ} during the reaction. However, this stabilization is greater for RIFZ as the LUMO becomes the HOMO-1. The HOMO-LUMO gap of 0.1337 hartree for this complex is also higher than the one (0.1022 hartree) computed for I_{FZ} . Thus, a lower stabilization of the LUMO and a larger HOMO-LUMO gap are consistent with a lower activity of this complex. Indeed, the barrier for the cleavage of the P-Ot from RII (23.5 kcal/mol) is 7.7 kcal/mol higher than that from R^I_{FZ}. Additionally, the corresponding transition state (TIFZ in Figure S18a) is stabilized by two hydrogen bonds, whereas T_{FZ}^{I} is stabilized by three (Figure 2). In the homobinuclear R_{CC}^{II} , and R_{CC}^{II} , unlike the corresponding R^I_{ZZ} and R^I_{CC} , there is no $\pi - \pi$ interaction between BDNPP and the ligand. The metal-metal and metal-ligand distances are also shorter in the reactants formed by the complexes of II than those formed by the complexes of I (Table S2). Furthermore, the locations of the two hydroxyl groups in these systems are found to be influenced by the nature of the metal ions, i.e., Fe(-OH) and μ -OH in R^{II}_{FZ} , two μ -OH in R^{II}_{ZZ} , and Cu1(-OH) and Cu2(-OH) in R^{II}_{CC} . The same locations of these groups are also observed in the two corresponding reactants of I, i.e., R^I_{FZ} and R^I_{ZZ} (Figures 2 and 3). However, the Cu2(-OH) arrangement in R^{I}_{CC} is different than two μ -OH arrangement in R^{II}_{CC} (Figure 4 and Figure S18c). The charges on the O² and O¹ atoms of RII and RII cc largely remain unchanged during the reaction, whereas only the charge on the O1 atom of the

nucleophile decreases by 0.21e in the $R^{II}_{ZZ} \rightarrow T^{II}_{ZZ}$ transformation. The charge on the nucleophile-providing Zn1 also increases by 0.04e. In the $R^{II}_{CC} \rightarrow T^{II}_{CC}$ process, the charge on the nucleophile-providing Cu2 also increases by 0.04e. In RII CC, the HOMO is located on the bridging phenolate linker (Figure S19). However, in comparison to R^{1}_{CC} , the LUMO+1 is positioned on the leaving group of the substrate. In the $R^{II}_{CC} \rightarrow T^{II}_{CC}$ transition, the LUMO+1 and not the LUMO of R^{II}_{CC} gets populated and mixes with other orbitals to stabilize to the HOMO-2. On the other hand, the LUMO converts into the HOMO-1 in the $R^I_{CC} \rightarrow T^I_{CC}$ transition. The barrier of 7.0 kcal/mol in R^{II}_{ZZ} is only slightly higher, by 0.7 kcal/mol, than the barrier of 6.3 kcal/mol in R¹₇₇. However, as expected, the corresponding barrier (9.6 kcal/mol) in R^{II}_{CC} is actually lower by 1.8 kcal/mol than the one computed for RI_{CC} (11.4 kcal/mol). Although the HOMO-LUMO+1 energy gap of 0.1174 hartree for R^{II}_{CC} is greater than the corresponding HOMO–LUMO gap of 0.0861hartree for R^{I}_{CC} , it is still more active than R^{I}_{CC} . This increase in activity is attributed to the greater orbital stabilization. Nonetheless, barriers for complexes of II follow the same order $[II_{ZZ}$ (7.0 kcal/mol) $< II_{CC}$ (9.6 kcal/mol) $< II_{FZ}$ (23.5 kcal/ mol)] as those observed for their counterparts with ligand I. These correspond well to the strength of the nucleophile in terms of the metal-nucleophile distance in their reactants $(Zn_1^{\ II}-O^1=2.08\ \text{Å}>Cu_1^{\ II}-O^1=1.90\ \text{Å}>Fe^{III}-O^1=1.84\ \text{Å}$ in $\mathbf{R^{II}}_{ZZ}$, $\mathbf{R^{II}}_{CC}$, and $\mathbf{R^{II}}_{FZ}$, respectively). Additionally, the scissile P-Ot bond is the most (1.68 Å) and least (1.66 Å) activated in R^{II}_{CC} and R^{II}_{FZ} , respectively (Table S2).

These results illustrate that the nature of the metal ions determines the activities of their complexes with ligands I and II. For instance, the Zn-Zn variants of both ligands (I_{ZZ} and II_{ZZ}) are the most active. However, whereas R^I_{FZ} is significantly more active than R^I_{FZ} , R^I_{ZZ} and R^I_{ZZ} are equally active, and R^I_{CC} is slightly more reactive than R^I_{CC} in the mechanistic model using the DA pathway. Additionally, barriers for the WA mechanism follow exactly the same pattern for both types of ligands (Figures S15 and S20). These results indicate that binuclear metal complexes with asymmetric (I) ligands are not more active than their symmetric (II) counterparts for all of the metal combinations analyzed.

3.5. Effects of Different Nucleophiles. Because Fe^{MI} -Zn^{II} and Zn^{II} -Zn^{II} core-containing complexes of I have been found to be more reactive than the corresponding complexes of II, only systems (I_{FZ} , I_{ZZ} , and I_{CC}) with ligand I are used to study the effects of different nucleophiles. As discussed above, different metal ion combinations can utilize a distinct nucleophile in the reaction, *i.e.*, Fe1-OH by R^{I}_{FZ} , μ -OH by R^{I}_{ZZ} , and Cu2-OH by R^{I}_{CC} . Here, the effects of different nucleophiles (μ -OH, terminal-OH, and $-O_2H_3$) and their combinations (one terminal and one μ -OH groups, only one μ -OH group, and only an $-O_2H_3$ group) in the models are investigated using the DA mechanism. The influence of the coordination numbers of the metal ions on the energetics of this mechanism is also explored.

3.5.1. Bridging (μ -OH) Nucleophile. Because the bridging hydroxyl (μ -OH) has been proposed as a potential nucleophile in previous studies, ^{17,118,119} its role in the P-O^t bond cleavage is investigated. In $\mathbf{R}^{\mathrm{I}}_{\mathrm{FZ}}$, the μ -O²H² is asymmetric and more strongly bound to Fe^{III} than Zn^{II} as a result of the higher charge (2.69e) of the former (Fe^{III}-O² = 1.97 Å and Zn^{II}-O² = 2.04 Å). In the transition state ($\mathbf{T}^{\mathrm{I}}_{\mathrm{FZ}}$), μ -O²H² completely loses its coordination with Zn^{II} during the attack on the P

electrophile and shifts completely toward Fe^{III} (Figure S21). In $\mathbf{T}^{\mathbf{I}\boldsymbol{\mu}}_{FZ}$, both $-\mathbf{O}^{1}\mathbf{H}^{1}$ and $-\mathbf{O}^{2}\mathbf{H}^{2}$ groups are bound only to Fe^{III}. The barrier for this process is significantly higher (by 20.2 kcal/mol) than the barrier computed for the terminal Fe^{III}bound -OH nucleophile, i.e., 36.0 kcal/mol in R^I_{FZ}. This could be due to the energetic penalty associated with the translocation of the strongly bound μ -O²H² to a terminal position and the concomitant weak stabilization of T^{μ}_{FZ} . The barrier using this bridging nucleophile is also higher (by 12.4 and 15.9 kcal/mol, respectively) in R^{I}_{ZZ} and R^{I}_{CC} . In the corresponding transition states ($T^{I\mu}_{ZZ}$ and $T^{I\mu}_{CC}$ in Figure S21), unlike $T^{I\mu}_{FZ}$, the -O²H² is, however, bound to both metal ions. This interaction lowers its nucleophilicity in comparison to its terminal counterpart. Although much higher in energy, the activities of these complexes utilizing the bridging nucleophile follow the same order $(I_{ZZ} > I_{CC} > I_{FZ})$ as the reactivities using the terminal hydroxyl nucleophile.

The removal of the terminal M1-bound -O¹H¹ group from the model (single μ -O¹H¹ group) creates a vacant site on this metal site. That allows BDNPP to coordinate to both metal ions in a bidentate fashion in the $R^{I\text{-}t}_{FZ}$ and $R^{I\text{-}t}_{ZZ}$ reactants, but it remains bound only to Cu2 in R^{I-t}_{CC} (Figure S22 and Table S3). However, as observed in the DA mechanism (Figure 2), the scissile bond of the substrate also becomes stronger by 0.4-0.7 Å in these reactants in comparison to its free form (Table S4). The bond cleavage in this model occurs with a 9.0 kcal/mol lower barrier than in the previous model, but it is still 11.2 kcal/mol higher than that computed using the Fe^{III}-bound terminal hydroxyl group (Figure 2). A similar pattern is observed for the homobinuclear ZnII-ZnII and CuII-CuII systems; i.e., the barriers of R^{I-t}_{ZZ} and R^{I-t}_{CC} are lower by 7.9 and 5.7 kcal/mol, respectively, but still remain higher than in the original models used in Figures 3 and 4. Additionally, all transition states $(T^{I-t}_{FZ}, T^{I-t}_{ZZ})$ and T^{I-t}_{CC} in this model are four-membered (Fe-O⁵-P-O² in Figure S22) and more strained than in the corresponding $T^{I}_{\ FZ}$, $T^{I}_{\ ZZ}$, and $T^{I}_{\ CC}$ transition states. The combined results suggest that the bridging hydroxyl group is a stronger nucleophile in the absence of a terminal hydroxyl group, but overall, it is still weaker than the terminal hydroxyl group.

3.5.2. $-O_2H_3$ ($H_2O\cdots OH$) Nucleophile. In the most stable conformation using the -O₂H₃ nucleophile, the M1-bound O¹H¹⁻ group and M2-coordinated H₂O form a hydrogen bond with each other, i.e., $[(M1)OH^-\cdots H_2O(M2)]$ (Figure S23). The reactants of the hetero- (R^{IH}_{FZ}) and homobinuclear $(R^{IH}_{\ ZZ} \ \text{and} \ R^{IH}_{\ CC})$ metal ion combinations adopt different conformations and vary in aspects of the mechanism (Figures S23 and S24). For instance, in R^{IH}_{FZ}, BDNPP coordinates to both metal ions, and the P-Ot bond gets strengthened by 0.07 Å (Figure S23 and Table S5). In this reactant, the attack by the -O₂H₃ nucleophile takes place with a barrier of 17.2 kcal/mol, which is only 1.4 kcal/mol higher than the barrier of 15.8 kcal/ mol calculated utilizing the terminal hydroxyl group for this complex (Figure 2). In contrast, in the homobinuclear R^{IH}_{ZZ} and \mathbf{R}^{IH}_{CC} , BDNPP coordinates only to M2, and the hydroxyl (-O¹H¹) group also shifts to the same site, leading to a variation of the DA mechanism. Here, the M2-bound hydroxyl functions as a base and activates the M1-bound water to be the nucleophile that subsequently cleaves the P-Ot bond. From R^{IH}_{ZZ} , the barrier for this process is 10.2 kcal/mol, which is 3.9 kcal/mol higher than the barrier using the terminal hydroxide. Similarly, the corresponding barrier from R^{IH}_{CC} is 16.5 kcal/ mol, which is 5.1 kcal/mol higher than the barrier for the

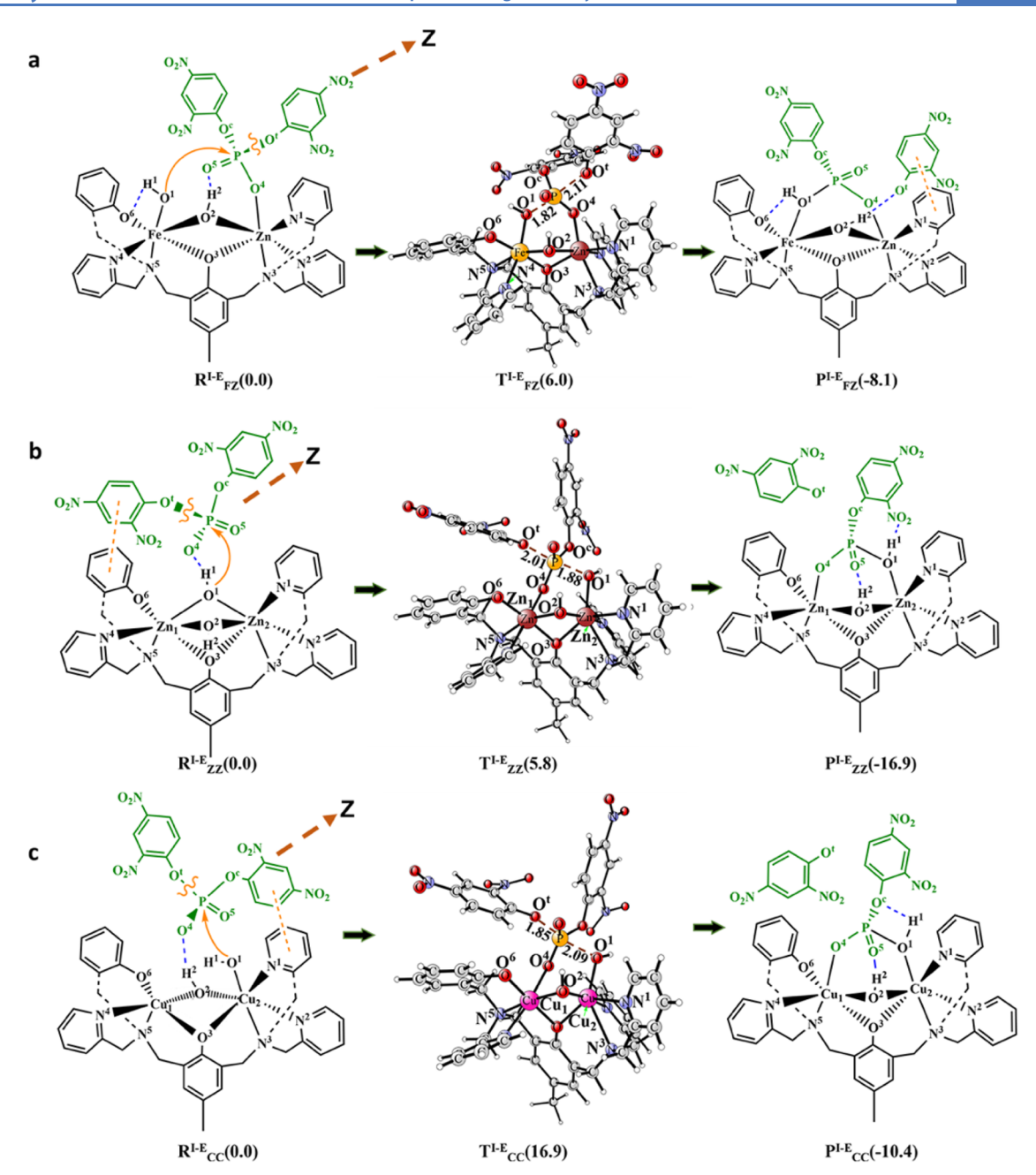


Figure 5. Optimized structures for (a) I_{FZ} , (b) I_{ZZ} , and (c) I_{CC} in the DA pathway in the presence of an external electric field (the Z axis represents the direction of the field).

system using the terminal hydroxide nucleophile (Figure 4). The trend in the barriers (*i.e.*, 10.2, 16.5, and 17.2 kcal/mol for R^{IH}_{ZZ} , R^{IH}_{CC} , and R^{IH}_{FZ} , respectively) is attributed to the decreasing nucleophilicity of the hydroxyl group in these complexes. The metal–nucleophile distance and P-O^t bond length also follow the same trend (Table S5). These results suggest that the $-O_2H_3$ nucleophile is stronger than the bridging one but weaker than the terminal hydroxyl group.

3.6. Effect of *para*-Substitution on the Substrate. The methyl (-CH₃) group in the *para* position of the centered phenolate is substituted with the chemically distinct -Cl and -NO₂ groups to study the effect of this substitution on the energetics of the DA mechanism for the dizinc reactant formed with ligand $I(I_{ZZ})$. I_{ZZ} is found to be the most active complex in all mechanisms investigated in this study. Among these

substituents, the -CH₃ group is an electron-donating group, -Cl is a moderate electron-withdrawing group, and -NO₂ is a strong electron-withdrawing group. In the corresponding reactants (\mathbf{R}^{I}_{ZZ} , \mathbf{R}^{IC}_{ZZ} , and \mathbf{R}^{IN}_{ZZ}) for the -CH₃, -Cl, and -NO₂ substituents, respectively, the M1-M2 distance increases and the M2–nucleophile (\mathbf{Z}_{12} -O¹) bond becomes slightly shorter (Table S6) in presence of the -Cl and -NO₂ groups. The decrease in the \mathbf{Z}_{12} -O¹ distance follows the order -CH₃ > -Cl > -NO₂. Thus, the nucleophilicity of the -O¹H¹ group decreases, and consequently, the barrier increases from -CH₃ to -NO₂ (*i.e.*, 6.3, 7.9, and 9.2 kcal/mol for -CH₃, -Cl, and -NO₂, respectively; Figure S25). Thus, in summary, a strong correlation is observed between the barrier and electron-donating and -withdrawing potential of the *para* substituents.

Table 3. Computed Energy Barriers for Different Complexes of Ligand I

complex	nucleophile	para substituent	pathway	rate-limiting barrier (kcal/mol)	measured barrier (kcal/mol)
I_{FZ}	Fe-OH	-CH ₃	DA-trans	15.8	20.1
	Fe-OH	-CH ₃	DA-cis	25.0	
	Fe-OH	-CH ₃	SA	35.6	
	H_2O	-CH ₃	WA	22.6	
	μ -OH (HO-Fe-OH-Zn)	-CH ₃	DA (μ-OH)	36.0	
	μ -OH (Fe-OH-Zn)	-CH ₃	DA (μ-OH)	27.0	
	$Fe-H_3O_2-Zn$	-CH ₃	$DA-H_3O_2$	17.2	
	Fe-OH	-CH ₃	DA (electric field)	6.0	
I_{ZZ}	Zn-OH	-CH ₃	DA-trans	6.3	
	Zn-OH	-CH ₃	DA-trans	15.0	
	Zn-OH	-CH ₃	SA	29.2	
	H_2O	-CH ₃	WA	14.3	
	μ -OH (Zn-OH-Zn-OH)	-CH ₃	DA (μ-OH)	18.7	
	μ -OH (Zn-OH-Zn)	-CH ₃	DA (μ-OH)	10.8	
	$Zn-H_3O_2-Zn$	$-CH_3$	$DA-H_3O_2$	10.2	
	Zn-OH	-CH ₃	AS	13.1	
	Zn-OH	-Cl	DA	7.9	
	Zn-OH	$-NO_2$	DA	9.2	
	Zn-OH	-CH ₃	DA (electric field)	5.8	
I_{CC}	Cu-OH	-CH ₃	DA-trans	11.4	
	Cu-OH	-CH ₃	DA-cis	25.7	
	Cu-OH	-CH ₃	SA	28.9	
	H2O	-CH ₃	WA	24.2	
	μ -OH (Cu-OH-Cu-OH)	-CH ₃	DA (μ-OH)	27.3	
	μ -OH (Cu-OH-Cu)	-CH ₃	DA (μ-OH)	21.6	
	Cu-H ₃ O ₂ -Cu	-CH ₃	$DA-H_3O_2$	16.5	
	Cu-OH	-CH ₃	DA (electric field)	16.9	

3.7. Effect of an External Electric Field. It has previously been demonstrated that an external electric field can be used as an accessory catalyst or an inhibitor for a reaction. 141,169 To study its possible effect on the reactions catalyzed by heteroand homobinuclear reactants of ligand I, an external electric field (Z + 10) was applied along the reaction axis in the DA mechanism (Figure 5). The field introduces noticeable changes in the geometry of the reactant $(R^{I\text{-}E}_{FZ})$ in comparison to R^{I}_{FZ} . For instance, the M1-M2 distance becomes shorter by 0.05 Å and the M2-BDNPP bond (Zn-O4) elongates by 0.09 Å (Figure 5, Table 1, and Table S7). Because the scissile P-Ot in R^{I-E}_{FZ} is not on the reaction axis, its length (1.67 Å) remains unchanged. However, in the transition state T^{I-E}_{FZ}, the scissile bond lies on the reaction axis, and it is elongated by 0.11 Å when compared to the corresponding transition state in the absence of the electric field (T^{I}_{FZ}) . Additionally, the Zcomponent of the dipole moment changes from +7.0 to -12.3D in the $R^{I-E}_{FZ} \rightarrow T^{I-E}_{FZ}$ transformation (Table S8). Thus, the increased nucleophilicity of the Fe^{III}-bound hydroxyl group (-O¹H¹ in Figure 5a) and activation of the P-O^t bond in the transition state significantly lower the barrier for this mechanism by 9.8 to 6.0 kcal/mol. However, in the reactant (R^{I-E}_{ZZ}) of the dizinc core-containing complex, neither the terminal nucleophile nor the scissile bond of the substrate is aligned with the reaction axis. Here, both the M1-M2 and P-Ot distances remain unchanged (Table 1 and Table S7). Additionally, the P-Ot bond is slightly (0.02 Å) stronger in the transition state $(T^{I-E}_{\ ZZ})$ in comparison to the corresponding bond in the absence of the electric field (TIZZ). Furthermore, in comparison to R^{I-E}_{FZ}, there is a much smaller

change in the dipole moment (+1.1 to -6.3 D; Table S8). As a result, the electric field exerts an almost negligible effect and only slightly decreases the barrier by 0.5 to 5.8 kcal/mol (Figure 5). On the other hand, in R^{I-E}_{CC} , the nucleophile is provided by the M2 site (Figure 5c). Thus, the electric field along the same axis is likely to exert the opposite effect and acts as an inhibitor by raising the barrier. As expected, in the transition state (T^{I-E}_{CC}) for this system, the P-O^t bond is significantly shorter (by 0.33 Å) than that in T^{I}_{CC} (Table 1 and Table S7). Additionally, in contrast to R^{I-E}_{FZ} and R^{I-E}_{ZZ} , the signs of the dipole moments are reversed (*i.e.*, -4.6 to 0.8 D; Table S8). Consequently, the barrier for this complex is increased by 5.5 to 16.9 kcal/mol. These results clearly show that the introduction of an electric field along the same axis exerts different effects in these systems; *i.e.*, it lowers the barrier for R^{I}_{FZ} , retains it for R^{I}_{ZZ} , and increases it for R^{I}_{CC} .

4. CONCLUSIONS

In this DFT study, hydrolysis of BDNPP by hetero- and homobinuclear metal ion combinations of an asymmetric [I (I_{FZ} , I_{ZZ} , and I_{CC})] and symmetric [II (II_{FZ} , II_{ZZ} , and II_{CC})] ligand with Fe^{III} - Zn^{II} , Zn^{II} - Zn^{II} , and Cu^{II} - Cu^{II} cores has been investigated using four distinct mechanisms (DA, SA, WA, and AS). Additionally, the effects of different nucleophiles, coordination numbers, *para* substituents of the linker, and an external electric field on the energetics of these reactions have also been evaluated (Table 3).

Depending on their metal ion and ligand composition, these complexes adopt different geometries and electronic spin states. Additionally, the substrate binding modes of the three metal ion centers for both ligands are different. There is no Lewis acid activation of the substrate in these mechanisms, and hydrolysis is controlled by the nucleophilicity of the hydroxyl ion. The identity of the metal ions determines the activities of their complexes, and I_{ZZ} is found to be the most active complex in all mechanisms (Table 3 and Table S9). The geometries of the complexes of I and II are similar, but the substrate interacts with them in a distinct manner (Figures S6-S8). Overall, complexes formed with the asymmetric ligand I are more reactive than their symmetric counterparts formed by ligand II (Table 3). Among the four mechanisms, the DA mechanism is found to be energetically the most feasible. The terminal hydroxyl group is the strongest nucleophile in all cases, and the electron-donating -CH₃ group is a more suitable para substituent in the linker than the -Cl and -NO₂ groups (Table 3). The external electric field along the reaction axis exerted distinct effects on these systems by lowering the barrier for R^{I}_{FZ} , retaining it for R^{I}_{ZZ} , and increasing it for RI_{CC} (Table 3). In summary, this study has provided detailed insights into the contribution of the metal ion composition, ligand arrangement, and an external electric field to the reactivity of binuclear catalysts that mimic the active site of metallohydrolases. Furthermore, the study also probed the strength of possible nucleophiles that may initiate the hydrolytic reaction. Overall, the systems display flexibility in the molecular details of their mechanisms, dependent mostly on the identity of the metal ions present in the reactive core of the catalysts. This is in good agreement with mechanistic variations observed for different metal ion derivatives of metallohydrolases. 170-177 These insights may help in the design of more efficient synthetic analogues for a wide range of applications in medicine and biotechnology.

ASSOCIATED CONTENT

Data Availability Statement

All DFT calculations using these models were performed using the Gaussian 09 software. The details of these methods and software including relevant citations are provided in the Computational Details section. The Cartesian coordinates of all optimized structures are provided as Supporting Information materials.

Supporting Information

The Supporting Information is available free of charge at https://pubs.acs.org/doi/10.1021/acscatal.2c05758.

Figures S1-S25, Tables S1-S9, and Cartesian coordinates of all optimized structures (PDF)

AUTHOR INFORMATION

Corresponding Author

Rajeev Prabhakar — Department of Chemistry, University of Miami, Coral Gables, Florida 33146, United States; orcid.org/0000-0003-1137-1272; Phone: 305-284-9372; Email: rpr@miami.edu

Authors

Vindi M. Jayasinghe-Arachchige — Department of Chemistry, University of Miami, Coral Gables, Florida 33146, United States

Leonardo F. Serafim — Department of Chemistry, University of Miami, Coral Gables, Florida 33146, United States

Qiaoyu Hu — Department of Chemistry, University of Miami,
Coral Gables, Florida 33146, United States

Cihan Ozen – Department of Chemistry, University of Miami, Coral Gables, Florida 33146, United States

Sreerag N. Moorkkannur – Department of Chemistry, University of Miami, Coral Gables, Florida 33146, United States

Gerhard Schenk — School of Chemistry and Molecular Biosciences, The University of Queensland, Brisbane, Queensland 4072, Australia; orcid.org/0000-0001-8619-0631

Complete contact information is available at: https://pubs.acs.org/10.1021/acscatal.2c05758

Notes

The authors declare no competing financial interest.

ACKNOWLEDGMENTS

The authors declare no competing financial interests. This material is based upon work supported by a grant from the National Science Foundation (Grant CHE-2102563) to R.P. Computational resources from the University of Miami Institute for Data Science & Computing (IDSC) are greatly acknowledged. The Turkish Fulbright Commission award (Grant FY-2016-TR-SS-15) to C.O. is also acknowledged.

REFERENCES

- (1) Wilcox, D. E. Binuclear Metallohydrolases. Chem. Rev. 1996, 96, 2435–2458.
- (2) Sorokin, A. B. Recent progress on exploring μ -oxo bridged binuclear porphyrinoid complexes in catalysis and material science. *Coord. Chem. Rev.* **2019**, 389, 141–160.
- (3) Zhu, L.; dos Santos, O.; Koo, C. W.; Rybstein, M.; Pape, L.; Canary, J. W. Geometry-Dependent Phosphodiester Hydrolysis Catalyzed by Binuclear Copper Complexes. *Inorg. Chem.* **2003**, *42*, 7912–7920.
- (4) Schenk, G.; Mitić, N.; Gahan, L. R.; Ollis, D. L.; McGeary, R. P.; Guddat, L. W. Binuclear Metallohydrolases: Complex Mechanistic Strategies for a Simple Chemical Reaction. *Acc. Chem. Res.* **2012**, *45*, 1593–1603.
- (5) Ragunathan, K. G.; Schneider, H.-J. Binuclear Lanthanide Complexes as Catalysts for the Hydrolysis of Bis(p-nitrophenyl)-phosphate and Double-Stranded DNA. *Angew. Chem. Int. Ed. in English* 1996, 35, 1219–1221.
- (6) Mitić, N.; Smith, S. J.; Neves, A.; Guddat, L. W.; Gahan, L. R.; Schenk, G. The Catalytic Mechanisms of Binuclear Metallohydrolases. *Chem. Rev.* **2006**, *106*, 3338–3363.
- (7) Powers, D. C.; Ritter, T. Bimetallic Redox Synergy in Oxidative Palladium Catalysis. *Acc. Chem. Res.* **2012**, *45*, 840–850.
- (8) Yuen, H. F.; Marks, T. J. Synthesis and Catalytic Properties of Phenylene-Bridged Binuclear Organolanthanide Complexes. *Organometallics* **2008**, *27*, 155–158.
- (9) Gupta, K. C.; Sutar, A. K. Catalytic activities of Schiff base transition metal complexes. *Coord. Chem. Rev.* **2008**, 252, 1420–1450.
- (10) Tkatchouk, E.; Mankad, N. P.; Benitez, D.; Goddard, W. A.; Toste, F. D. Two Metals Are Better Than One in the Gold Catalyzed Oxidative Heteroarylation of Alkenes. *J. Am. Chem. Soc.* **2011**, *133*, 14293–14300.
- (11) Sinha, S.; Mirica, L. M. Electrocatalytic O2 Reduction by an Organometallic Pd(III) Complex via a Binuclear Pd(III) Intermediate. ACS Catal. 2021, 11, 5202–5211.
- (12) Sinha, W.; Mahammed, A.; Fridman, N.; Gross, Z. Water Oxidation Catalysis by Mono- and Binuclear Iron Corroles. *ACS Catal.* **2020**, *10*, 3764–3772.
- (13) Klähn, M.; Garland, M. V. On the Mechanism of the Catalytic Binuclear Elimination Reaction in Hydroformylation Systems. *ACS Catal.* **2015**, *5*, 2301–2316.

- (14) Hetterscheid, D. G. H.; Chikkali, S. H.; de Bruin, B.; Reek, J. N. H. Binuclear Cooperative Catalysts for the Hydrogenation and Hydroformylation of Olefins. *ChemCatChem* **2013**, *5*, 2785–2793.
- (15) Pye, D. R.; Mankad, N. P. Bimetallic catalysis for C-C and C-X coupling reactions. *Chem. Sci.* **2017**, *8*, 1705–1718.
- (16) Xu, B.; Jiang, W.; Liu, X.; Liu, F.; Xiang, Z. Remarkable reactivity of alkoxide/acetato-bridged binuclear copper(II) complex as artificial carboxylesterase. *JBIC*, *J. Biol. Inorg. Chem.* **2017**, 22, 625–635.
- (17) Erxleben, A. Interactions of copper complexes with nucleic acids. *Coord. Chem. Rev.* **2018**, *360*, 92–121.
- (18) Lanznaster, M.; Neves, A.; Bortoluzzi, A. J.; Szpoganicz, B.; Schwingel, E. New FeIIIZnII Complex Containing a Single Terminal Fe-Ophenolate Bond as a Structural and Functional Model for the Active Site of Red Kidney Bean Purple Acid Phosphatase. *Inorg. Chem.* **2002**, *41*, 5641–5643.
- (19) Das, B.; Daver, H.; Singh, A.; Singh, R.; Haukka, M.; Demeshko, S.; Meyer, F.; Lisensky, G.; Jarenmark, M.; Himo, F.; et al. A Heterobimetallic FeIIIMnII Complex of an Unsymmetrical Dinucleating Ligand: A Structural and Functional Model Complex for the Active Site of Purple Acid Phosphatase of Sweet Potato. *Eur. J. Inorg. Chem.* **2014**, 2014, 2204–2212.
- (20) Smith, S. J.; Peralta, R. A.; Jovito, R.; Horn, A.; Bortoluzzi, A. J.; Noble, C. J.; Hanson, G. R.; Stranger, R.; Jayaratne, V.; Cavigliasso, G.; Gahan, L. R.; Schenk, G.; Nascimento, O. R.; Cavalett, A.; Bortolotto, T.; Razzera, G.; Terenzi, H.; Neves, A.; Riley, M. J. Spectroscopic and Catalytic Characterization of a Functional FeIIIFeII Biomimetic for the Active Site of Uteroferrin and Protein Cleavage. *Inorg. Chem.* **2012**, *51*, 2065–2078.
- (21) Jarenmark, M.; Kappen, S.; Haukka, M.; Nordlander, E. Symmetrical and unsymmetrical dizinc complexes as models for the active sites of hydrolytic enzymes. *Dalton Trans.* **2008**, *8*, 993–996.
- (22) Williams, N. H.; Takasaki, B.; Wall, M.; Chin, J. Structure and nuclease activity of simple dinuclear metal complexes: quantitative dissection of the role of metal ions. *Acc. Chem. Res.* **1999**, 32, 485–493.
- (23) Breslow, R. Artificial enzymes. John Wiley & Sons 2005, 63-88.
- (24) Lowther, W. T.; Matthews, B. W. Metalloaminopeptidases: Common Functional Themes in Disparate Structural Surroundings. *Chem. Rev.* **2002**, *102*, 4581–4608.
- (25) Williams, N. H.; Cheung, W.; Chin, J. Reactivity of Phosphate Diesters Doubly Coordinated to a Dinuclear Cobalt(III) Complex: Dependence of the Reactivity on the Basicity of the Leaving Group. *J. Am. Chem. Soc.* **1998**, *120*, 8079–8087.
- (26) Williams, N. H.; Chin, J. Metal-ion catalysed phosphate diester transesterification: quantifying double Lewis-acid activation. *Chem. Commun.* **1996**, *2*, 131–132.
- (27) Dupureur, C. M. One is enough: insights into the two-metal ion nuclease mechanism from global analysis and computational studies. *Metallomics* **2010**, *2*, 609–620.
- (28) Bazzicalupi, C.; Bencini, A.; Bonaccini, C.; Giorgi, C.; Gratteri, P.; Moro, S.; Palumbo, M.; Simionato, A.; Sgrignani, J.; Sissi, C.; et al. Tuning the Activity of Zn(II) Complexes in DNA Cleavage: Clues for Design of New Efficient Metallo-Hydrolases. *Inorg. Chem.* **2008**, 47, 5473–5484.
- (29) Qian, J.; Gu, W.; Liu, H.; Gao, F.; Feng, L.; Yan, S.; Liao, D.; Cheng, P. The first dinuclear copper(ii) and zinc(ii) complexes containing novel Bis-TACN: syntheses, structures, and DNA cleavage activities. *Dalton Trans.* **2007**, *10*, 1060–1066.
- (30) Gahan, L. R.; Smith, S. J.; Neves, A.; Schenk, G. Phosphate Ester Hydrolysis: Metal Complexes As Purple Acid Phosphatase and Phosphotriesterase Analogues. *Eur. J. Inorg. Chem.* **2009**, 2009, 2745–2758.
- (31) Joshi, T.; Graham, B.; Spiccia, L. Macrocyclic Metal Complexes for Metalloenzyme Mimicry and Sensor Development. *Acc. Chem. Res.* **2015**, *48*, 2366–2379.
- (32) Dalle, K. E.; Meyer, F. Modelling Binuclear Metallobiosites: Insights from Pyrazole-Supported Biomimetic and Bioinspired Complexes. *Eur. J. Inorg. Chem.* **2015**, 2015, 3391–3405.

- (33) Hu, Q.; Jayasinghe-Arachchige, V. M.; Sharma, G.; Serafim, L. F.; Paul, T. J.; Prabhakar, R. Mechanisms of peptide and phosphoester hydrolysis catalyzed by two promiscuous metalloenzymes (insulin degrading enzyme and glycerophosphodiesterase) and their synthetic analogues. *Wiley Interdiscip. Rev. Comput. Mol. Sci.* **2020**, *10*, No. e1466.
- (34) Erxleben, A. Mechanistic Studies of Homo- and Heterodinuclear Zinc Phosphoesterase Mimics: What Has Been Learned? *Front. Chem.* **2019**, 7, 1–22.
- (35) Piovezan, C.; Jovito, R.; Bortoluzzi, A. J.; Terenzi, H.; Fischer, F. L.; Severino, P. C.; Pich, C. T.; Azzolini, G. G.; Peralta, R. A.; Rossi, L. M.; et al. Heterodinuclear FeIIIZnII-Bioinspired Complex Supported on 3-Aminopropyl Silica. Efficient Hydrolysis of Phosphate Diester Bonds. *Inorg. Chem.* **2010**, *49*, 2580–2582.
- (36) Peralta, R. A.; Bortoluzzi, A. J.; de Souza, B.; Jovito, R.; Xavier, F. R.; Couto, R. A. A.; Casellato, A.; Nome, F.; Dick, A.; Gahan, L. R.; Schenk, G.; Hanson, G. R.; de Paula, F. C. S.; Pereira-Maia, E. C.; de Machado, P. S.; Severino, P. C.; Pich, C.; Bortolotto, T.; Terenzi, H.; Castellano, E. E.; Neves, A.; Riley, M. J. Electronic Structure and Spectro-Structural Correlations of FeIIIZnII Biomimetics for Purple Acid Phosphatases: Relevance to DNA Cleavage and Cytotoxic Activity. *Inorg. Chem.* **2010**, *49*, 11421–11438.
- (37) Silva, G. A. d. S.; Amorim, A. L.; Souza, B. d.; Gabriel, P.; Terenzi, H.; Nordlander, E.; Neves, A.; Peralta, R. A. Synthesis and characterization of $FeIII(\mu\text{-OH})$ ZnII complexes: effects of a second coordination sphere and increase in the chelate ring size on the hydrolysis of a phosphate diester and DNA. *Dalton Trans.* **2017**, 46, 11380–11394.
- (38) Karsten, P.; Neves, A.; Bortoluzzi, A. J.; Lanznaster, M.; Drago, V. Synthesis, Structure, Properties, and Phosphatase-Like Activity of the First Heterodinuclear FeIIIMnII Complex with the Unsymmetric Ligand H2BPBPMP as a Model for the PAP in Sweet Potato. *Inorg. Chem.* **2002**, *41*, 4624–4626.
- (39) Schenk, G.; Peralta, R. A.; Batista, S. C.; Bortoluzzi, A. J.; Szpoganicz, B.; Dick, A. K.; Herrald, P.; Hanson, G. R.; Szilagyi, R. K.; Riley, M. J.; Gahan, L. R.; Neves, A. Probing the role of the divalent metal ion in uteroferrin using metal ion replacement and a comparison to isostructural biomimetics. *JBIC, J. Biol. Inorg. Chem.* **2007**, *13*, 139–155.
- (40) Xavier, F. R.; Neves, A.; Casellato, A.; Peralta, R. A.; Bortoluzzi, A. J.; Szpoganicz, B.; Severino, P. C.; Terenzi, H.; Tomkowicz, Z.; Ostrovsky, S.; Haase, W.; Ozarowski, A.; Krzystek, J.; Telser, J.; Schenk, G.; Gahan, L. R. Unsymmetrical FeIIICoII and GaIIICoII Complexes as Chemical Hydrolases: Biomimetic Models for Purple Acid Phosphatases (PAPs). *Inorg. Chem.* **2009**, *48*, 7905–7921.
- (41) Lengyel, Z.; Rufo, C. M.; Moroz, Y. S.; Makhlynets, O. V.; Korendovych, I. V. Copper-Containing Catalytic Amyloids Promote Phosphoester Hydrolysis and Tandem Reactions. *ACS Catal.* **2018**, *8*, 59–62.
- (42) Wang, Y.; Yang, L.; Wang, M.; Zhang, J.; Qi, W.; Su, R.; He, Z. Bioinspired Phosphatase-like Mimic Built from the Self-Assembly of De Novo Designed Helical Short Peptides. *ACS Catal.* **2021**, *11*, 5839–5849.
- (43) Liu, S.; Du, P.; Sun, H.; Yu, H.-Y.; Wang, Z.-G. Bioinspired Supramolecular Catalysts from Designed Self-Assembly of DNA or Peptides. ACS Catal. 2020, 10, 14937–14958.
- (44) Kuah, E.; Toh, S.; Yee, J.; Ma, Q.; Gao, Z. Enzyme Mimics: Advances and Applications. *Chem. Eur. J.* **2016**, 22, 8404–8430.
- (45) Raynal, M.; Ballester, P.; Vidal-Ferran, A.; van Leeuwen, P. W. N. M. Supramolecular catalysis. Part 2: artificial enzyme mimics. *Chem. Soc. Rev.* **2014**, *43*, 1734–1787.
- (46) Meeuwissen, J.; Reek, J. N. H. Supramolecular catalysis beyond enzyme mimics. *Nat. Chem.* **2010**, *2*, 615–621.
- (47) Xu, H.; Cao, W.; Zhang, X. Selenium-Containing Polymers: Promising Biomaterials for Controlled Release and Enzyme Mimics. *Acc. Chem. Res.* **2013**, *46*, 1647–1658.
- (48) Wiester, M. J.; Ulmann, P. A.; Mirkin, C. A. Enzyme Mimics Based Upon Supramolecular Coordination Chemistry. *Angew. Chem., Int. Ed.* **2011**, *50*, 114–137.

- (49) Dong, Z.; Luo, Q.; Liu, J. Artificial enzymes based on supramolecular scaffolds. *Chem. Soc. Rev.* **2012**, *41*, 7890–7908.
- (50) Lin, Y.; Ren, J.; Qu, X. Catalytically Active Nanomaterials: A Promising Candidate for Artificial Enzymes. *Acc. Chem. Res.* **2014**, *47*, 1097–1105.
- (51) Silva, D.-A.; Yu, S.; Ulge, U. Y.; Spangler, J. B.; Jude, K. M.; Labão-Almeida, C.; Ali, L. R.; Quijano-Rubio, A.; Ruterbusch, M.; Leung, I.; et al. De novo design of potent and selective mimics of IL-2 and IL-15. *Nature* **2019**, *565*, 186–191.
- (52) Lu, Y.; Yeung, N.; Sieracki, N.; Marshall, N. M. Design of functional metalloproteins. *Nature* **2009**, *460*, 855–862.
- (53) Deuss, P. J.; den Heeten, R.; Laan, W.; Kamer, P. C. J. Bioinspired Catalyst Design and Artificial Metalloenzymes. *Chem. Eur. J.* **2011**, *17*, 4680–4698.
- (54) Wei, H.; Wang, E. Nanomaterials with enzyme-like characteristics (nanozymes): next-generation artificial enzymes. *Chem. Soc. Rev.* **2013**, *42*, 6060–6093.
- (55) Tolbert, A. E.; Ervin, C. S.; Ruckthong, L.; Paul, T. J.; Jayasinghe-Arachchige, V. M.; Neupane, K. P.; Stuckey, J. A.; Prabhakar, R.; Pecoraro, V. L. Heteromeric three-stranded coiled coils designed using a Pb(ii)(Cys)3 template mediated strategy. *Nat. Chem.* **2020**, *12*, 405–411.
- (56) Zhang, T.; Ozbil, M.; Barman, A.; Paul, T. J.; Bora, R. P.; Prabhakar, R. Theoretical Insights into the Functioning of Metallopeptidases and Their Synthetic Analogues. *Acc. Chem. Res.* **2015**, *48*, 192–200.
- (57) Serafim, L. F.; Wang, L.; Rathee, P.; Yang, J.; Frenk Knaul, H. S.; Prabhakar, R. Remediation of environmentally hazardous organophosphates by artificial metalloenzymes. *Curr. Opin. Green Sustain. Chem.* **2021**, 32, No. 100529.
- (58) Katz, M. J.; Klet, R. C.; Moon, S.-Y.; Mondloch, J. E.; Hupp, J. T.; Farha, O. K. One Step Backward Is Two Steps Forward: Enhancing the Hydrolysis Rate of UiO-66 by Decreasing [OH–]. ACS Catal. 2015, 5, 4637–4642.
- (59) Luo, H.-B.; Castro, A. J.; Wasson, M. C.; Flores, W.; Farha, O. K.; Liu, Y. Rapid, Biomimetic Degradation of a Nerve Agent Simulant by Incorporating Imidazole Bases into a Metal—Organic Framework. *ACS Catal.* **2021**, *11*, 1424—1429.
- (60) Zhang, X.; Liu, X.; Phillips, D. L.; Zhao, C. Mechanistic Insights Into the Factors That Influence the DNA Nuclease Activity of Mononuclear Facial Copper Complexes Containing Hetero-Substituted Cyclens. ACS Catal. 2016, 6, 248–257.
- (61) Chin, J.; Kim, H.-J. Artificial Enzymes. Wiley-Vch: Weinheim, 2005.
- (62) Weston, J. Mode of Action of Bi- and Trinuclear Zinc Hydrolases and Their Synthetic Analogues. *Chem. Rev.* **2005**, *105*, 2151–2174.
- (63) Lipscomb, W. N. N. S.; Sträter, N. Recent Advances in Zinc Enzymology. *Chem. Rev.* **1996**, *96*, 2375–2434.
- (64) Mareque-Rivas, J. C.; Prabaharan, R.; Martin de Rosales, R. T. Relative importance of hydrogen bonding and coordinating groups in modulating the zinc-water acidity. *Chem. Commun.* **2004**, *1*, 76–77.
- (65) Camargo, T. P.; Neves, A.; Peralta, R. A.; Chaves, C.; Maia, E. C. P.; Lizarazo-Jaimes, E. H.; Gomes, D. A.; Bortolotto, T.; Norberto, D. R.; Terenzi, H.; Tierney, D. L.; Schenk, G. Second-Sphere Effects in Dinuclear FeIIIZnII Hydrolase Biomimetics: Tuning Binding and Reactivity Properties. *Inorg. Chem.* **2018**, *57*, 187–203.
- (66) Daver, H.; Das, B.; Nordlander, E.; Himo, F. Theoretical Study of Phosphodiester Hydrolysis and Transesterification Catalyzed by an Unsymmetric Biomimetic Dizinc Complex. *Inorg. Chem.* **2016**, *55*, 1872–1882.
- (67) Maxwell, C. I.; Mosey, N. J.; Stan Brown, R. DFT Computational Study of the Methanolytic Cleavage of DNA and RNA Phosphodiester Models Promoted by the Dinuclear Zn(II) Complex of 1,3-Bis(1,5,9-triazacyclododec-1-yl)propane. *J. Am. Chem. Soc.* 2013, 135, 17209–17222.
- (68) Collins-Wildman, D. L.; Kim, M.; Sullivan, K. P.; Plonka, A. M.; Frenkel, A. I.; Musaev, D. G.; Hill, C. L. Buffer-Induced Acceleration

- and Inhibition in Polyoxometalate-Catalyzed Organophosphorus Ester Hydrolysis. ACS Catal. 2018, 8, 7068–7076.
- (69) Guo, W.; Lv, H.; Sullivan, K. P.; Gordon, W. O.; Balboa, A.; Wagner, G. W.; Musaev, D. G.; Bacsa, J.; Hill, C. L. Broad-Spectrum Liquid- and Gas-Phase Decontamination of Chemical Warfare Agents by One-Dimensional Heteropolyniobates. *Angew. Chem., Int. Ed.* **2016**, *55*, 7403–7407.
- (70) Aboelnga, M. M.; Wetmore, S. D. Unveiling a Single-Metal-Mediated Phosphodiester Bond Cleavage Mechanism for Nucleic Acids: A Multiscale Computational Investigation of a Human DNA Repair Enzyme. *J. Am. Chem. Soc.* **2019**, *141*, 8646–8656.
- (71) López, X.; Carbó, J. J.; Bo, C.; Poblet, J. M. Structure, properties and reactivity of polyoxometalates: a theoretical perspective. *Chem. Soc. Rev.* **2012**, *41*, 7537–7571.
- (72) Florián, J.; Warshel, A. Phosphate Ester Hydrolysis in Aqueous Solution: Associative versus Dissociative Mechanisms. *J. Phys. Chem.* B 1998. 102. 719–734.
- (73) Ghanem, E.; Li, Y.; Xu, C.; Raushel, F. M. Characterization of a phosphodiesterase capable of hydrolyzing EA 2192, the most toxic degradation product of the nerve agent VX. *Biochemistry* **2007**, *46*, 9032–9040.
- (74) Knowles, J. R. Enzyme-catalyzed phosphoryl transfer reactions. *Annu. Rev. Biochem.* **1980**, *49*, 877–919.
- (75) Lassila, J. K.; Zalatan, J. G.; Herschlag, D. Biological phosphoryl-transfer reactions: understanding mechanism and catalysis. *Annu. Rev. Biochem.* **2011**, *80*, 669–702.
- (76) Cowan, J. A. Metal Activation of Enzymes in Nucleic Acid Biochemistry. *Chem. Rev.* **1998**, *98*, 1067–1088.
- (77) Kuimelis, R. G.; McLaughlin, L. W. Mechanisms of ribozyme-mediated RNA cleavage. *Chem. Rev.* **1998**, 98, 1027–1044.
- (78) Kottur, J.; Nair, D. T. Pyrophosphate hydrolysis is an intrinsic and critical step of the DNA synthesis reaction. *Nucleic Acids Res.* **2018**, *46*, 5875–5885.
- (79) Klumpp, K.; Hang, J. Q.; Rajendran, S.; Yang, Y.; Derosier, A.; Wong Kai In, P.; Overton, H.; Parkes, K. E. B.; Cammack, N.; Martin, J. A. Two-metal ion mechanism of RNA cleavage by HIV RNase H and mechanism-based design of selective HIV RNase H inhibitors. *Nucleic Acids Res.* **2003**, *31*, 6852–6859.
- (80) Shaw-Reid, C. A.; Feuston, B.; Munshi, V.; Getty, K.; Krueger, J.; Hazuda, D. J.; Parniak, M. A.; Miller, M. D.; Lewis, D. Dissecting the Effects of DNA Polymerase and Ribonuclease H Inhibitor Combinations on HIV-1 Reverse-Transcriptase Activities. *Biochemistry* **2005**, *44*, 1595–1606.
- (81) Daumann, L. J.; Larrabee, J. A.; Ollis, D.; Schenk, G.; Gahan, L. R. Immobilization of the enzyme GpdQ on magnetite nanoparticles for organophosphate pesticide bioremediation. *J. Inorg. Biochem.* **2014**, *131*, 1–7.
- (82) Ghanem, E.; Raushel, F. M. Detoxification of organophosphate nerve agents by bacterial phosphotriesterase. *Toxicol. Appl. Pharmacol.* **2005**, 207, 459–470.
- (83) Chandra, M.; Sachdeva, A.; Silverman, S. K. DNA-catalyzed sequence-specific hydrolysis of DNA. *Nat. Chem. Biol.* **2009**, *5*, 718–720.
- (84) Pedroso, M. M.; Ely, F.; Mitić, N.; Carpenter, M. C.; Gahan, L. R.; Wilcox, D. E.; Larrabee, J. L.; Ollis, D. L.; Schenk, G. Comparative investigation of the reaction mechanisms of the organophosphate-degrading phosphotriesterases from Agrobacterium radiobacter (OpdA) and Pseudomonas diminuta (OPH). *JBIC, J. Biol. Inorg. Chem.* **2014**, *19*, 1263–1275.
- (85) Feder, D.; Mohd-Pahmi, S. H.; Hussein, W. M.; Guddat, L. W.; McGeary, R. P.; Schenk, G. Rational Design of Potent Inhibitors of a Metallohydrolase Using a Fragment-Based Approach. *ChemMedChem* **2021**, *16*, 3342–3359.
- (86) Newmark, J. Nerve Agents. Neurologist 2007, 13, 20-32.
- (87) Pedroso, M. M.; Hine, D.; Hahn, S.; Chmielewicz, W. M.; Diegel, J.; Gahan, L.; Schenk, G. Pesticide degradation by immobilised metalloenzymes provides an attractive avenue for bioremediation. *EFB Bioecon. J.* **2021**, *1*, No. 100015.

- (88) Daumann, L. J.; Schenk, G.; Ollis, D. L.; Gahan, L. R. Spectroscopic and mechanistic studies of dinuclear metallohydrolases and their biomimetic complexes. *Dalton Trans.* **2014**, *43*, 910–928.
- (89) Parkin, G. Synthetic Analogues Relevant to the Structure and Function of Zinc Enzymes. *Chem. Rev.* **2004**, *104*, 699–768.
- (90) Luong, T. K. N.; Shestakova, P.; Mihaylov, T. T.; Absillis, G.; Pierloot, K.; Parac-Vogt, T. N. Multinuclear Diffusion NMR Spectroscopy and DFT Modeling: A Powerful Combination for Unraveling the Mechanism of Phosphoester Bond Hydrolysis Catalyzed by Metal-Substituted Polyoxometalates. *Chem. Eur. J.* 2015, 21, 4428–4439.
- (91) Sträter, N.; Lipscomb, W. N.; Klabunde, T.; Krebs, B. Enzymatische Acyl-und Phosphoryltransferreaktionen unter Beteiligung von zwei Metallionen. *Am. Ethnol.* **1996**, *108*, 2158–2191.
- (92) Kövári, E.; Krämer, R. Rapid Phosphodiester Hydrolysis by an Ammonium-Functionalized Copper(II) Complex. A Model for the Cooperativity of Metal Ions and NH-Acidic Groups in Phosphoryl Transfer Enzymes. J. Am. Chem. Soc. 1996, 118, 12704–12709.
- (93) Komiyama, M.; Kina, S.; Matsumura, K.; Sumaoka, J.; Tobey, S.; Lynch, V. M.; Anslyn, E. Trinuclear Copper(II) Complex Showing High Selectivity for the Hydrolysis of 2'-5' over 3'-5' for UpU and 3'-5' over 2'-5' for ApA Ribonucleotides. *J. Am. Chem. Soc.* **2002**, 124, 13731–13736.
- (94) Schiller, A.; Scopelliti, R.; Benmelouka, M.; Severin, K. Highly Cross-linked Polymers Containing N,N',N"-Chelate Ligands for the Cu(II)-Mediated Hydrolysis of Phosphoesters. *Inorg. Chem.* **2005**, *44*, 6482–6492.
- (95) Comba, P.; Gahan, L. R.; Hanson, G. R.; Westphal, M. Phosphatase reactivity of a dicopper (ii) complex of a patellamide derivative—possible biological functions of cyclic pseudopeptides. *Chem. Commun.* **2012**, *48*, 9364–9366.
- (96) Yang, M.-Y.; Iranzo, O.; Richard, J. P.; Morrow, J. R. Solvent Deuterium Isotope Effects on Phosphodiester Cleavage Catalyzed by an Extraordinarily Active Zn(II) Complex. J. Am. Chem. Soc. 2005, 127, 1064–1065.
- (97) Vichard, C.; Kaden, T. A. Phosphate and phosphonate ester hydrolysis promoted by dinuclear metal complexes. *Inorg. Chim. Acta* **2002**, 337, 173–180.
- (98) Buchholz, R. R.; Etienne, M. E.; Dorgelo, A.; Mirams, R. E.; Smith, S. J.; Chow, S. Y.; Hanton, L. R.; Jameson, G. B.; Schenk, G.; Gahan, L. R. A structural and catalytic model for zinc phosphoesterases. *Dalton Trans.* **2008**, *43*, 6045–6054.
- (99) Gao, H.; Ke, Z.; DeYonker, N. J.; Wang, J.; Xu, H.; Mao, Z.-W.; Phillips, D. L.; Zhao, C. Dinuclear Zn(II) Complex Catalyzed Phosphodiester Cleavage Proceeds via a Concerted Mechanism: A Density Functional Theory Study. *J. Am. Chem. Soc.* **2011**, *133*, 2904–2915.
- (100) Daumann, L. J.; Dalle, K. E.; Schenk, G.; McGeary, R. P.; Bernhardt, P. V.; Ollis, D. L.; Gahan, L. R. The role of Zn-OR and Zn-OH nucleophiles and the influence of para-substituents in the reactions of binuclear phosphatase mimetics. *Dalton Trans.* **2012**, *41*, 1695–1708.
- (101) Daumann, L. J.; Marty, L.; Schenk, G.; Gahan, L. R. Asymmetric zinc(ii) complexes as functional and structural models for phosphoesterases. *Dalton Trans.* **2013**, *42*, 9574–9584.
- (102) Das, B.; Daver, H.; Pyrkosz-Bulska, M.; Persch, E.; Barman, S. K.; Mukherjee, R.; Gumienna-Kontecka, E.; Jarenmark, M.; Himo, F.; Nordlander, E. A dinuclear zinc(II) complex of a new unsymmetric ligand with an N(5)O(2) donor set: a structural and functional model for the active site of zinc phosphoesterases. *J. Inorg. Biochem.* **2014**, 132, 6–17.
- (103) Montagner, D.; Gandin, V.; Marzano, C.; Erxleben, A. Phosphate Diester Cleavage, DNA Interaction and Cytotoxic Activity of a Bimetallic Bis(1,4,7-triazacyclononane) Zinc Complex. *Eur. J. Inorg. Chem.* **2014**, 2014, 4084–4092.
- (104) Zhang, X.; Zheng, X.; Phillips, D. L.; Zhao, C. Mechanistic investigation of the cleavage of phosphodiester catalyzed by a symmetrical oxymine-based macrocyclic dinuclear zinc complex: a DFT study. *Dalton Trans.* **2014**, *43*, 16289–16299.

- (105) Massoud, S. S.; Ledet, C. C.; Junk, T.; Bosch, S.; Comba, P.; Herchel, R.; Hosek, J.; Travnicek, Z.; Fischer, R. C.; Mautner, F. A. Dinuclear metal(ii)-acetato complexes based on bicompartmental 4-chlorophenolate: syntheses, structures, magnetic properties, DNA interactions and phosphodiester hydrolysis. *Dalton Trans.* **2016**, *45*, 12933–12950.
- (106) Das, B.; Daver, H.; Pyrkosz-Bulska, M.; Gumienna-Kontecka, E.; Himo, F.; Nordlander, E. An Unsymmetric Ligand with a N5O2 Donor Set and Its Corresponding Dizinc Complex: A Structural and Functional Phosphoesterase Model. *Eur. J. Inorg. Chem.* **2018**, 2018, 4004–4013.
- (107) Iranzo, O.; Elmer, T.; Richard, J. P.; Morrow, J. R. Cooperativity between Metal Ions in the Cleavage of Phosphate Diesters and RNA by Dinuclear Zn(II) Catalysts. *Inorg. Chem.* **2003**, 42, 7737–7746.
- (108) Yang, M.-Y.; Richard, J. P.; Morrow, J. R. Substrate specificity for catalysis of phosphodiester cleavage by a dinuclear Zn(ii) complex. *Chem. Commun.* **2003**, 22, 2832–2833.
- (109) Bazzicalupi, C.; Bencini, A.; Berni, E.; Bianchi, A.; Fornasari, P.; Giorgi, C.; Valtancoli, B. Zn(II) Coordination to Polyamine Macrocycles Containing Dipyridine Units. New Insights into the Activity of Dinuclear Zn(II) Complexes in Phosphate Ester Hydrolysis. *Inorg. Chem.* **2004**, *43*, 6255–6265.
- (110) Jarenmark, M.; Csapó, E.; Singh, J.; Wöckel, S.; Farkas, E.; Meyer, F.; Haukka, M.; Nordlander, E. Unsymmetrical dizinc complexes as models for the active sites of phosphohydrolases. *Dalton Trans.* **2010**, *39*, 8183–8194.
- (111) Bazzicalupi, C.; Bencini, A.; Bianchi, A.; Fusi, V.; Giorgi, C.; Paoletti, P.; Valtancoli, B.; Zanchi, D. Carboxy and Phosphate Esters Cleavage with Mono-and Dinuclear Zinc (II) Macrocyclic Complexes in Aqueous Solution. Crystal Structure of [Zn2L1 (μ -PP) 2 (MeOH) 2](ClO4) 2 (L1=[30] aneN6O4, PP-= Diphenyl Phosphate). *Inorg. Chem.* 1997, 36, 2784–2790.
- (112) Zastrow, M. L.; Pecoraro, V. L. Designing Hydrolytic Zinc Metalloenzymes. *Biochemistry* **2014**, *53*, 957–978.
- (113) Khare, S. D.; Kipnis, Y.; Greisen, P., Jr.; Takeuchi, R.; Ashani, Y.; Goldsmith, M.; Song, Y.; Gallaher, J. L.; Silman, I.; Leader, H.; Sussman, J. L.; Stoddard, B. L.; Tawfik, D. S.; Baker, D. Computational redesign of a mononuclear zinc metalloenzyme for organophosphate hydrolysis. *Nat. Chem. Biol.* **2012**, *8*, 294–300.
- (114) Hänsch, R.; Mendel, R. R. Physiological functions of mineral micronutrients (Cu, Zn, Mn, Fe, Ni, Mo, B, Cl). *Curr. Opin. Plant Biol.* **2009**, *12*, 259–266.
- (115) Song, W. J.; Tezcan, F. A. A designed supramolecular protein assembly with in vivo enzymatic activity. *Science* **2014**, *346*, 1525–1528.
- (116) Xu, D.; Cui, Q.; Guo, H. Quantum mechanical/molecular mechanical studies of zinc hydrolases. *Int. Rev. Phys. Chem.* **2014**, 33, 1–41
- (117) Neves, A.; Lanznaster, M.; Bortoluzzi, A. J.; Peralta, R. A.; Casellato, A.; Castellano, E. E.; Herrald, P.; Riley, M. J.; Schenk, G. An Unprecedented FeIII(μ -OH)ZnII Complex that Mimics the Structural and Functional Properties of Purple Acid Phosphatases. *J. Am. Chem. Soc.* **2007**, *129*, 7486–7487.
- (118) Montagner, D.; Gandin, V.; Marzano, C.; Erxleben, A. DNA damage and induction of apoptosis in pancreatic cancer cells by a new dinuclear bis(triazacyclonane) copper complex. *J. Inorg. Biochem.* **2015**, *145*, 101–107.
- (119) Smoukov, S. K.; Quaroni, L.; Wang, X.; Doan, P. E.; Hoffman, B. M.; Que, L. Electron— Nuclear Double Resonance Spectroscopic Evidence for a Hydroxo-Bridge Nucleophile Involved in Catalysis by a Dinuclear Hydrolase. *J. Am. Chem. Soc.* **2002**, *124*, 2595–2603.
- (120) Schenk, G.; Gahan, L. R.; Carrington, L. E.; Mitić, N.; Valizadeh, M.; Hamilton, S. E.; de Jersey, J.; Guddat, L. W. Phosphate forms an unusual tripodal complex with the Fe—Mn center of sweet potato purple acid phosphatase. *Proc. Natl. Acad. Sci.* **2005**, *102*, 273—278.
- (121) Fan, F.; Zheng, Y.; Zhang, Y.; Zheng, H.; Zhong, J.; Cao, Z. A Comprehensive Understanding of Enzymatic Degradation of the G-

- Type Nerve Agent by Phosphotriesterase: Revised Role of Water Molecules and Rate-Limiting Product Release. ACS Catal. 2019, 9, 7038–7051.
- (122) Hendry, P.; Sargeson, A. M. Metal ion promoted phosphate ester hydrolysis. Intramolecular attack of coordinated hydroxide ion. *J. Am. Chem. Soc.* **1989**, *111*, 2521–2527.
- (123) Mancin, F.; Tecilla, P. Zinc(ii) complexes as hydrolytic catalysts of phosphate diester cleavage: from model substrates to nucleic acids. *New J. Chem.* **2007**, *31*, 800–817.
- (124) Komiyama, M.; Takeda, N.; Shigekawa, H. Hydrolysis of DNA and RNA by lanthanide ions: mechanistic studies leading to new applications. *Chem. Commun.* **1999**, *16*, 1443–1451.
- (125) Duarte, F.; Åqvist, J.; Williams, N. H.; Kamerlin, S. C. L. Resolving Apparent Conflicts between Theoretical and Experimental Models of Phosphate Monoester Hydrolysis. *J. Am. Chem. Soc.* **2015**, 137, 1081–1093.
- (126) Zhang, T.; Zhu, X.; Prabhakar, R. Peptide Hydrolysis by Metal-Cyclen Complexes and Their Analogues: Insights from Theoretical Studies. *Organometallics* **2014**, *33*, 1925–1935.
- (127) Ferreira, D. E. C.; De Almeida, W. B.; Neves, A.; Rocha, W. R. Theoretical investigation of the reaction mechanism for the phosphate diester hydrolysis using an asymmetric dinuclear metal complex as a biomimetic model of the purple acid phosphatase enzyme. *Phys. Chem. Chem. Phys.* **2008**, *10*, 7039–7046.
- (128) Dal Peraro, M.; Llarrull, L. I.; Rothlisberger, U.; Vila, A. J.; Carloni, P. Water-Assisted Reaction Mechanism of Monozinc β -Lactamases. *J. Am. Chem. Soc.* **2004**, *126*, 12661–12668.
- (129) Jayasinghe-Arachchige, V. M.; Hu, Q.; Sharma, G.; Paul, T. J.; Lundberg, M.; Quinonero, D.; Parac-Vogt, T. N.; Prabhakar, R. Hydrolysis of chemically distinct sites of human serum albumin by polyoxometalate: A hybrid QM/MM (ONIOM) study. *J. Comput. Chem.* **2019**, *40*, 51–61.
- (130) Batebi, H.; Imhof, P. Phosphodiester hydrolysis computed for cluster models of enzymatic active sites. *Theor. Chem. Acc.* **2016**, *135*, 262.
- (131) De Vivo, M.; Dal Peraro, M.; Klein, M. L. Phosphodiester Cleavage in Ribonuclease H Occurs via an Associative Two-Metal-Aided Catalytic Mechanism. *J. Am. Chem. Soc.* **2008**, *130*, 10955–10962.
- (132) Zhou, X.; Zhang, X.-P.; Li, W.; Phillips, D. L.; Ke, Z.; Zhao, C. Electronic Effect on Bimetallic Catalysts: Cleavage of Phosphodiester Mediated by Fe(III)—Zn(II) Purple Acid Phosphatase Mimics. *Inorg. Chem.* **2020**, *59*, 12065—12074.
- (133) Coleman, F.; Hynes, M. J.; Erxleben, A. Ga(III) complexes as models for the M(III) site of purple acid phosphatase: ligand effects on the hydrolytic reactivity toward bis(2,4-dinitrophenyl) phosphate. *Inorg. Chem.* **2010**, *49*, 6725–6733.
- (134) Bertini, I.; Luchinat, C.; Rosi, M.; Sgamellotti, A.; Tarantelli, F. pKa of zinc-bound water and nucleophilicity of hydroxo-containing species. Ab initio calculations on models for zinc enzymes. *Inorg. Chem.* **1990**, *29*, 1460–1463.
- (135) Liu, C.; Wang, L. DNA hydrolytic cleavage catalyzed by synthetic multinuclear metallonucleases. *Dalton Trans.* **2009**, *2*, 227–239.
- (136) Bauer-Siebenlist, B.; Meyer, F.; Farkas, E.; Vidovic, D.; Dechert, S. Effect of Zn.··Zn Separation on the Hydrolytic Activity of Model Dizinc Phosphodiesterases. *Chem. Eur. J.* **2005**, *11*, 4349–4360.
- (137) Meyer, F. Clues to Dimetallohydrolase Mechanisms from Studies on Pyrazolate-Based Bioinspired Dizinc Complexes Experimental Evidence for a Functional Zn–O2H3–Zn Motif. *Eur. J. Inorg. Chem.* **2006**, 2006, 3789–3800.
- (138) Jeon, H.; Vazquez-Lima, H.; Jeong, H.; Cho, K.-B.; Hong, S. Mono- and dinuclear zinc complexes bearing identical bis-(thiosemicarbazone) ligand that exhibit alkaline phosphatase-like catalytic reactivity. *JBIC*, *J. Biol. Inorg. Chem.* **2022**, *27*, 37–47.
- (139) Shaik, S.; Ramanan, R.; Danovich, D.; Mandal, D. Structure and reactivity/selectivity control by oriented-external electric fields. *Chem. Soc. Rev.* **2018**, *47*, 5125–5145.

- (140) Shaik, S.; Mandal, D.; Ramanan, R. Oriented electric fields as future smart reagents in chemistry. *Nat. Chem.* **2016**, *8*, 1091–1098. (141) Che, F.; Gray, J. T.; Ha, S.; Kruse, N.; Scott, S. L.; McEwen, J.-S. Elucidating the Roles of Electric Fields in Catalysis: A Perspective. *ACS Catal.* **2018**, *8*, 5153–5174.
- (142) Chin, J. Developing artificial hydrolytic metalloenzymes by a unified mechanistic approach. *Acc. Chem. Res.* **1991**, *24*, 145–152.
- (143) Breslow, R.; Dong, S. D. Biomimetic Reactions Catalyzed by Cyclodextrins and Their Derivatives. *Chem. Rev.* **1998**, *98*, 1997–2012.
- (144) Breslow, R.; Zhang, B. Very fast ester hydrolysis by a cyclodextrin dimer with a catalytic linking group. *J. Am. Chem. Soc.* **1992**, *114*, 5882–5883.
- (145) Breslow, R.; Zhang, B. Cleavage of Phosphate Esters by a Cyclodextrin Dimer Catalyst That Binds the Substrates Together with La3+ and Hydrogen Peroxide. *J. Am. Chem. Soc.* **1994**, *116*, 7893–7894.
- (146) Breslow, R.; Zhang, X.; Xu, R.; Maletic, M.; Merger, R. Selective Catalytic Oxidation of Substrates That Bind to Metalloporphyrin Enzyme Mimics Carrying Two or Four Cyclodextrin Groups and Related Metallosalens. *J. Am. Chem. Soc.* **1996**, *118*, 11678–11679.
- (147) Suh, J. Model studies of metalloenzymes involving metal ions as Lewis acid catalysts. *Acc. Chem. Res.* **1992**, *25*, 273–279.
- (148) Suh, J. Synthetic artificial peptidases and nucleases using macromolecular catalytic systems. *Acc. Chem. Res.* **2003**, *36*, 562–570. (149) Guthrie, J. P. Hydration and dehydration of phosphoric acid derivatives: free energies of formation of the pentacoordinate intermediates for phosphate ester hydrolysis and of monomeric metaphosphate. *J. Am. Chem. Soc.* **1977**, *99*, 3991–4001.
- (150) Johnson, J. S.; Evans, D. A. Chiral Bis(oxazoline) Copper(II) Complexes: Versatile Catalysts for Enantioselective Cycloaddition, Aldol, Michael, and Carbonyl Ene Reactions. *Acc. Chem. Res.* **2000**, 33, 325–335.
- (151) Pfaltz, A. Chiral semicorrins and related nitrogen heterocycles as ligands in asymmetric catalysis. *Acc. Chem. Res.* **1993**, *26*, 339–345.
- (152) Frisch, M.; Trucks, G.; Schlegel, H.; Scuseria, G.; Robb, M.; Cheeseman, J.; Scalmani, G.; Barone, V.; Mennucci, B.; Petersson, G., et al. *Gaussian 09, rev. D.01*; Gaussian, Inc.: Wallingford, CT, 2009.
- (153) Adamo, C.; Barone, V. Exchange functionals with improved long-range behavior and adiabatic connection methods without adjustable parameters: The m PW and m PW1PW models. *J. Chem. Phys.* **1998**, *108*, 664–675.
- (154) Pritchard, B. P.; Altarawy, D.; Didier, B.; Gibson, T. D.; Windus, T. L. modeling, New basis set exchange: An open, up-to-date resource for the molecular sciences community. *J. Chem. Inf. Model.* **2019**, *59*, 4814–4820.
- (155) Hay, P. J.; Wadt, W. R. Ab initio effective core potentials for molecular calculations. Potentials for the transition metal atoms Sc to Hg. J. Chem. Phys. 1985, 82, 270–283.
- (156) Liu, Q.; Liu, X.; Shi, C.; Zhang, Y.; Feng, X.; Cheng, M.-L.; Su, S.; Gu, J. A copper-based layered coordination polymer: synthesis, magnetic properties and electrochemical performance in supercapacitors. *Dalton Trans.* **2015**, *44*, 19175–19184.
- (157) Feng, X.; Gu, J.; Xie, Y.; King, R. B.; Schaefer, H. F. Homoleptic Carbonyls of the Second-Row Transition Metals: Evaluation of Hartree— Fock and Density Functional Theory Methods. J. Chem. Theory Comput. 2007, 3, 1580–1587.
- (158) Deng, L.; Ziegler, T. The determination of Intrinsic Reaction Coordinates by density functional theory. *Int. J. Quantum Chem.* **1994**, 52, 731–765.
- (159) Grimme, S.; Ehrlich, S.; Goerigk, L. Effect of the damping function in dispersion corrected density functional theory. *J. Comput. Chem.* **2011**, 32, 1456–1465.
- (160) Cances, E.; Mennucci, B.; Tomasi, J. A new integral equation formalism for the polarizable continuum model: Theoretical background and applications to isotropic and anisotropic dielectrics. *J. Chem. Phys.* **1997**, *107*, 3032–3041.

- (161) Blomberg, M. R. The structure of the oxidized state of cytochrome c oxidase-experiments and theory compared. *J. Inorg. Biochem.* **2020**, *206*, No. 111020.
- (162) Foster, J. P.; Weinhold, F. Natural hybrid orbitals. *J. Am. Chem. Soc.* **1980**, *102*, 7211–7218.
- (163) Becke, A. D. Density-functional exchange-energy approximation with correct asymptotic behavior. *Phys. Rev. A: At., Mol., Opt. Phys.* **1988**, 38, 3098–3100.
- (164) Zhao, Y.; Truhlar, D. G. A new local density functional for main-group thermochemistry, transition metal bonding, thermochemical kinetics, and noncovalent interactions. *J. Chem. Phys.* **2006**, *125*, 194101.
- (165) Zhao, Y.; Truhlar, D. G. The M06 suite of density functionals for main group thermochemistry, thermochemical kinetics, non-covalent interactions, excited states, and transition elements: two new functionals and systematic testing of four M06-class functionals and 12 other functionals. *Theor. Chem. Acc.* 2008, 120, 215–241.
- (166) Sharma, G.; Jayasinghe-Arachchige, V. M.; Hu, Q.; Schenk, G.; Prabhakar, R. Effect of Chemically Distinct Substrates on the Mechanism and Reactivity of a Highly Promiscuous Metallohydrolase. *ACS Catal.* **2020**, *10*, 3684–3696.
- (167) Hadler, K. S.; Tanifum, E. A.; Yip, S. H.-C.; Mitić, N.; Guddat, L. W.; Jackson, C. J.; Gahan, L. R.; Nguyen, K.; Carr, P. D.; Ollis, D. L.; Hengge, A. C.; Larrabee, J. A.; Schenk, G. Substrate-Promoted Formation of a Catalytically Competent Binuclear Center and Regulation of Reactivity in a Glycerophosphodiesterase from Enterobacter aerogenes. J. Am. Chem. Soc. 2008, 130, 14129–14138.
- (168) Serafim, L. F.; Jayasinghe-Arachchige, V. M.; Wang, L.; Prabhakar, R. Promiscuous Catalytic Activity of a Binuclear Metallohydrolase: Peptide and Phosphoester Hydrolyses. *J. Chem. Inf. Model.* **2022**, *62*, 2466–2480.
- (169) Meir, R.; Chen, H.; Lai, W.; Shaik, S. Oriented electric fields accelerate Diels—Alder reactions and control the endo/exo selectivity. *ChemPhysChem* **2010**, *11*, 301–310.
- (170) Twitchett, M. B.; Schenk, G.; Aquino, M. A. S.; Yiu, D. T. Y.; Lau, T.-C.; Sykes, A. G. Reactivity of MII Metal-Substituted Derivatives of Pig Purple Acid Phosphatase (Uteroferrin) with Phosphate. *Inorg. Chem.* **2002**, *41*, 5787–5794.
- (171) Mitić, N.; Hadler, K. S.; Gahan, L. R.; Hengge, A. C.; Schenk, G. The Divalent Metal Ion in the Active Site of Uteroferrin Modulates Substrate Binding and Catalysis. *J. Am. Chem. Soc.* **2010**, *132*, 7049–7054.
- (172) Ely, F.; Hadler, K. S.; Gahan, L. R.; Guddat, L. W.; Ollis, D. L.; Schenk, G. The organophosphate-degrading enzyme from Agrobacterium radiobacter displays mechanistic flexibility for catalysis. *Biochem. J.* **2010**, *432*, 565–573.
- (173) Daumann, L. J.; McCarthy, B. Y.; Hadler, K. S.; Murray, T. P.; Gahan, L. R.; Larrabee, J. A.; Ollis, D. L.; Schenk, G. Promiscuity comes at a price: Catalytic versatility vs efficiency in different metal ion derivatives of the potential bioremediator GpdQ. *Biochim. Biophys. Acta, Proteins Proteomics* **2013**, *1834*, 425–432.
- (174) Miraula, M.; Whitaker, J. J.; Schenk, G.; Mitić, N. β-Lactam antibiotic-degrading enzymes from non-pathogenic marine organisms: a potential threat to human health. *JBIC*, J. Biol. Inorg. Chem. **2015**, 20, 639–651.
- (175) Pedroso, M. M.; Larrabee, J. A.; Ely, F.; Gwee, S. E.; Mitić, N.; Ollis, D. L.; Gahan, L. R.; Schenk, G. CaII Binding Regulates and Dominates the Reactivity of a Transition-Metal-Ion-Dependent Diesterase from Mycobacterium tuberculosis. *Chem. Eur. J.* **2016**, 22, 999–1009
- (176) Selleck, C.; Larrabee, J. A.; Harmer, J.; Guddat, L. W.; Mitić, N.; Helweh, W.; Ollis, D. L.; Craig, W. R.; Tierney, D. L.; Monteiro Pedroso, M.; et al. AIM-1: An Antibiotic-Degrading Metallohydrolase That Displays Mechanistic Flexibility. *Chem. Eur. J.* **2016**, 22, 17704–17714.
- (177) Miraula, M.; Schenk, G.; Mitić, N. Promiscuous metallo- β -lactamases: MIM-1 and MIM-2 may play an essential role in quorum sensing networks. *J. Inorg. Biochem.* **2016**, *162*, 366–375.

□ Recommended by ACS

Ligand-Based Redox: Catalytic Applications and Mechanistic Aspects

Kirti Singh, Debashis Adhikari, et al.

OCTOBER 12, 2022

READ 🗹

Nitrogen-Neighbored Single-Cobalt Sites Enable Heterogeneous Oxidase-Type Catalysis

Qi Zhang, Yong Cao, et al.

FEBRUARY 09, 2023

JOURNAL OF THE AMERICAN CHEMICAL SOCIETY

READ 🗹

Highly Adaptive Nature of Group 15 *Tris*(quinolyl) Ligands—Studies with Coinage Metals

Álvaro García-Romero, Dominic S. Wright, et al.

MARCH 08, 2023

INORGANIC CHEMISTRY

READ 🗹

Mechanistic Investigations into the Selective Reduction of Oxygen by a Multicopper Oxidase T3 Site-Inspired Dicopper Complex

Phebe H. van Langevelde, Dennis G. H. Hetterscheid, et al.

APRIL 12, 2023

ACS CATALYSIS

READ 🗹

Get More Suggestions >